

Fundamentals and applications of the photocatalytic treatment for the removal of industrial organic pollutants and effects of operational parameters: A review

Rajendra Singh Thakur,^{1,a)} Rubina Chaudhary,^{2,b)} and Chandan Singh^{1,c)}

¹Research Scholar, School of Energy and Environmental Studies, Devi Ahilya University, Takshshila Campus, Khandawa Road, Indore, Madhya Pradesh 452017, India

²Reader, School of Energy and Environmental Studies, Devi Ahilya University, Takshshila Campus, Khandawa Road, Indore, Madhya Pradesh 452017, India

(Received 8 February 2010; accepted 2 July 2010; published online 26 July 2010)

Photocatalysis process, as an environmental application, is a relatively novel subject with tremendous potential in the near future. A number of studies determine the economic viability of applying various ultraviolet advanced oxidation processes for the purpose of degradation and destroying of various pollutant solutions. The present paper reviews the treatment of hazardous wastewater bearing organic compounds and the effects of various parameters such as pH, initial concentration, mass of catalyst, wavelength, light intensity, electron acceptor, temperature, etc., with the treatment cost for different reactor type. This study investigates the effect of various types of waste-water treatment parameters and the treatment cost for various designs of photocatalytic reactors, using both solar and artificial light, have been proposed for their different types of pollutants. © 2010 American Institute of Physics.

[doi:10.1063/1.3467511]

I. INTRODUCTION

Photocatalytic oxidation is a potential method for the treatment of organic contaminants and has received significant interest and research.¹ This research includes more advanced oxidation process, which can be powered by irradiation light with a wavelength longer than 300 nm, homogeneous and heterogeneous with photo-Fenton photocatalysis using TiO₂, with and without addition of oxidants.² It is based mainly on the oxidative reactivity of HO· radicals generated by various methods such as O₃/UV, H₂O₂/UV, H₂O₂/visible, O₃/H₂O₂/UV photolysis, photoassisted and TiO₂-mediated and UV/TiO₂/Na₂S₂O₈,³ (NH₄)₂S₂O₈/UV, (NH₄)₂S₂O₈,⁴ H₂O₂/Fe²⁺, UV/H₂O₂/Fe (Ref. 2) photocatalysis processes.⁵ Literature review has established that practically any pollutant that includes aliphatic, aromatics, dyes, surfactants, pesticides, and herbicides can be completely mineralized by this process into harmless substances.⁶ By heterogeneous photocatalysis, dispersed solid particles absorb larger fractions of the UV spectrum efficiently and generate chemical oxidants.⁷ Many researchers have examined some methods for fixing TiO₂ on supporting materials including glass beads, fiberglass, silica, and zeolite.⁸ The initial interest in the heterogeneous photocatalysis was started when discovered in 1972 the photochemical splitting of water into hydrogen and oxygen with TiO₂.⁹ The oxidation-reduction behavior of species in contact with TiO₂ determines whether the material will be photo-oxidized or photoreduced.¹⁰ Furthermore, a number of publications examined the effect of solution matrix, inorganic oxidants, and other

^{a)}Electronic mail: rsthakur.sees@gmail.com.

^{b)}Author to whom correspondence should be addressed. Tel.: +91-731-2460309. FAX: +91-731-2460737. Electronic mail: rubina_chaudhary@yahoo.com.

^{c)}Electronic mail: csingh07_sees@yahoo.com.

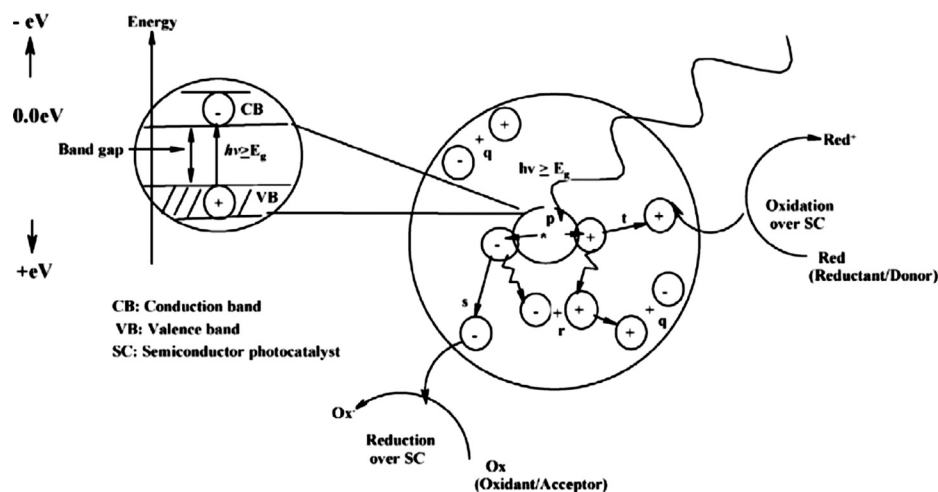


FIG. 1. Schematic photophysical and photochemical processes over photon activated semiconductor cluster (p) photogeneration of electron/hole pair, (q) surface recombination, (r) recombination in the bulk, (s) diffusion of acceptor and reduction on the surface of semi-conductors (SC), and (t) oxidation of donor on the surface of SC particle.

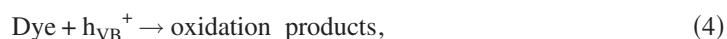
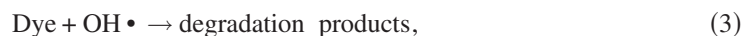
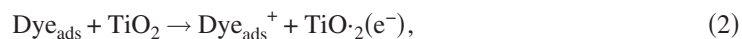
chemicals on the photocatalytic degradation of organic contaminants in water. The optimum conditions obtained (concentration of the catalyst, pH of solution, type of catalyst, and light intensity) were subsequently applied for the detoxification of the actual industrial wastewater.

II. MECHANISM OF TITANIA-ASSISTED PHOTOCATALYTIC

Many elementary mechanistic processes have been described in the photocatalytic degradation of organic compounds over TiO₂ surface.¹¹ Such as TiO₂ absorbs a photon of energy equal to or greater than its band-gap width, an electron may be promoted from the valence band to the conduction band (e⁻_{cb}) leaving behind an electron vacancy or “hole” in the valence band (h⁺_{vb}) shown in Fig. 1.

For a more detailed discussion of the interaction of light with matter, the reader may consult some of the standard sources on photochemistry. Table I includes the representative photochemical processes.¹²

These oxidative reactions would result in the direct absorption of light by the dye, which can further lead to charge injection from the excited state of the dye to the conduction band of the semiconductor as summarized³ in the following:



III. PHOTOCATALYTIC PROPERTIES

The ideal photocatalyst should possess the following properties: (i) photoactivity, (ii) biological and chemical inertness, (iii) stability toward photocorrosion, (iv) suitability toward visible or

TABLE I. Basic methods of photochemical processes.

Photochemical processes	Photochemical equations	Comments	Reference
Direct photochemistry	$A \xrightarrow{h\nu} A^* \xrightarrow{(O_2, H_2O)} \text{Products}$	Light is absorbed by a compound A and the excited state A* goes on to react with oxygen and water to be mineralized to carbon dioxide or to produce small molecules.	12
Photochemistry of molecules	$A + \text{Surface} \xrightarrow{(h\nu)} A_{(\text{ads})} \xrightarrow{(O_2, H_2O)} A^*_{(\text{ads})} \rightarrow \text{Products}$	Molecules adsorbed on surfaces A _[ads] , where the adsorbed compound is excited to a reactive state by absorption of light and is degraded.	
Dye-sensitized oxidation	$D \xrightarrow{h\nu} D^* \xrightarrow{O_2(^3\Sigma_g^-)} \rightarrow O_2(^1\Sigma_g^-) \xrightarrow{H_2O, O_2} OH$	Sensitized formation of singlet oxygen, in the ¹ Σ _g state for example, or hydroxyl radical by energy transfer from an electronically excited donor D* to oxygen in the presence of water.	
Photocatalytic oxidation	$TiO_2(s) \xrightarrow{h\nu} TiO_2(s)^* \xrightarrow{O_2, H_2O} OH + HO_2$	Light of wavelength equal to or greater than the band gap of a semiconductor. The resulting valence band hole directly oxidizes a molecule or oxidizes water to produce an OH.	
Photo-Fenton	$Fe(OH)_{\text{aq}}^{+2} \xrightarrow{h\nu} Fe_{\text{aq}}^{+2} + OH$	Light absorption by iron (+3) hydroxo-complexes can result in electron transfer to give a hydroxyl radical and iron (+2).	

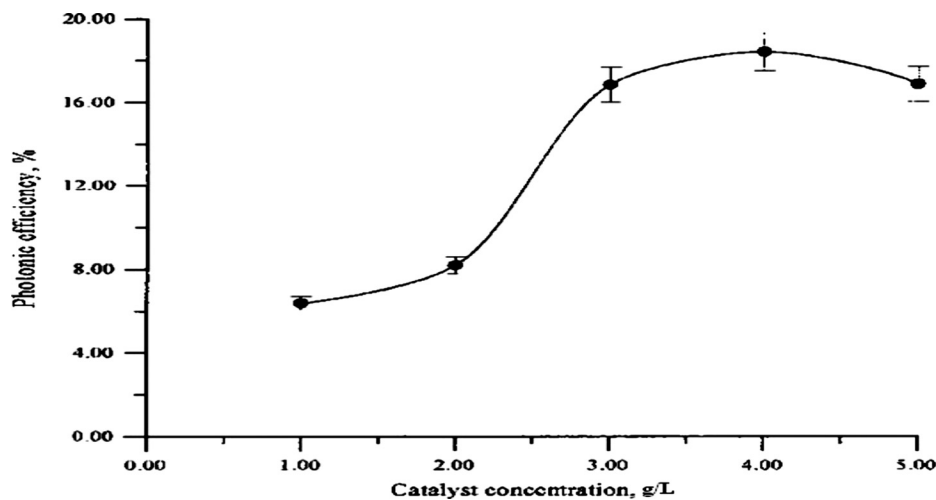


FIG. 2. Optimization of the photonic efficiency against different catalyst concentrations.

near UV light, (v) low cost, and (vi) lack of toxicity.⁹ Many materials such as TiO_2 , ZnO , MgO , ZrO_2 , CdS , MoS_2 , Fe_2O_3 , WO_3 , and their various combinations have been used for the degradation of organic pollutants.⁷ Among these, TiO_2 is the most widely used photocatalyst because of its good activity, high chemical stability, high ultraviolet adsorption, commercial availability, and inexpensiveness.¹³ In order to avoid the use of photocatalyst powder, efforts have been made to coat TiO_2 thin films on various substrates such as glass,¹⁴ indium-tin oxide glass,¹⁵ plastics,¹⁶ and polymers.¹⁷ TiO_2 thin films have been prepared by various techniques such as chemical vapor deposition,¹⁸ precipitation,¹⁹ flame synthesis,²⁰ and sol-gel dip coating.^{21,22} The photocatalytic water treatment with TiO_2 efficiently destroys many organic pollutants.²³ The photocatalytic degradation rate of different compounds depends on various parameters, such as temperature, pH, pollutant initial concentration, TiO_2 concentration, light intensity, chemical structure of the reactant, and physico-chemical and optical properties of the TiO_2 . Both crystal structures, anatase, and rutile are commonly used, with anatase showing a greater photocatalytic activity for most of the reactions. However, some studies showed that a mixture of anatase (70%–75%) and rutile (30%–25%) is more active than pure anatase.^{24,25}

A. Catalyst dose

It is observed that rate of reaction increases with increase in catalyst concentration and becomes constant above at a certain level. The reasons for this decrease in degradation rate are (i) aggregation of TiO_2 particles at high concentrations causing a decrease in the number of surface active sites and (ii) increase in opacity and light scattering of TiO_2 particles at high concentration leading to decrease.²⁶ By applying the optimal experimental conditions, obtained from the model potassium hydrogen phthalate (KHP) experiments, to the real wastewater samples, it was observed that 5 h irradiation of the wastewater in 3 g/l Degussa P25 was sufficient in order to degrade the organic pollutants in the investigated wastewater. This can be explained by the fact that at 3 g/l catalyst concentration, the maximum amount of incident light which could be absorbed was reached in the reactor used in this study. It is known from the literature that the particle size and the type of photocatalyst play a significant role in the degradation rate of organic pollutants shown in Fig. 2.²⁷ Many authors^{4,5,28–30} discussed this (Table II) by employing different concentration of the catalyst.

TABLE II. The effect of photocatalyst loading on organic pollutants.

Target of compound	Photocatalyst	Using catalyst loading	Result	Reference
Fast green FCF (1) and patent blue VF (2)	TiO ₂ , Hombikat UV100, and PC500	0.5–4 g/l and 1 g/l	Hombikat UV100 showed better photocatalytic activity for the degradation of dye 1, whereas Degussa P25 was better for dye 2.	4
Acridine orange and 3,6-diaminoacridine	TiO ₂ nanoparticles	TiO ₂ at 0.5 g/l and AO at 0.05 g/l	The photocatalytic degradation rate was found to increase with increasing TiO ₂ dosage.	5
Azo dye acid red 114	TiO ₂	20–80 mg/l	The degradation increases with an increase for catalyst up to a value of 40 mg/l and then decreases when catalyst concentration is increased.	8
Azo dye (AR27)	TiO ₂	50–400 mg/l	UV/TiO ₂ in the range of 0–300 mg/l. TiO ₂ dosage is probably due to an increased number of available adsorption and catalytic active site.	13
Diazo direct yellow 12 dye	TiO ₂	0.5–3.5 g/l	Rate increases with increase in catalyst concentration and becomes constant above a certain level, optimum catalyst for degradation is 2.0 g/l.	26
Portion H-cell dyes	TiO ₂	200–2000 mg/l	Decolorization rates increase in the TiO ₂ /UV process with the increase of TiO ₂ loading, especially up to about 1000 mg/l.	29
DNSDA, ANSDA, and DASDA	TiO ₂ , ferrous sulfate	TiO ₂ 2 g/l, Fe ²⁺ 0.05 mM, H ₂ O ₂ 15 mM	The removal of TOC increased with an increase in Fe ²⁺ concentration.	30
Chrysoidine Y (1)	TiO ₂ and zinc oxide	0.5–5 g/l	The mineralization and decomposition under investigation were found to increase with the increase in catalyst concentration.	31
1,4-dichlorobenzene	TiO ₂ , WO ₃ /TiO ₃ , and MoO ₃ /TiO ₂	3 mol % for WO ₃ and 2.5 mol % for MoOs	The acid number and strength increase with increasing mol % of WO ₃ or MoO ₃ until the surface of the TiO ₂ is effectively covered.	32

TABLE II. (Continued.)

Target of compound	Photocatalyst	Using catalyst loading	Result	Reference
C.I. reactive red 198	TiO ₂	0.5 g/l	Thereby reducing decolorization efficiency, the dye therefore has a UV-screening effect insofar as fewer photons reach the TiO ₂ surface as dye.	33
Naphthalene	TiO ₂	0–4 g/l (max 2.5g/l)	The existence of a threshold is attributed to a screening effect of TiO ₂ particles as their concentration increases.	34
Methylene blue (MB)	TiO ₂ nanofilm (5 nm average diameter)	Spray-coated with TiO ₂ solution	The adsorption mechanism provided significant contribution at pH 9 (higher than pzc of TiO ₂) when titanium surface is negatively charged.	35
Methylene blue (MB)	TiO ₂	100 mg	The kinetics of the photocatalytic process was independent of the total accumulated light energy absorbed by the TiO ₂ particles.	36
4BS azo dye	TiO ₂ anatase	0.5–6.0 g/l	With an increased catalyst dosage of enough power, the control step changes to the factor of a noncatalyst dosage.	37
Winery wastewater	TiO ₂	0–3 g/l	TiO ₂ had a shading effect on the light reaching in the reactor.	38
Pesticide pyridaben in CTAB	TiO ₂	0–4 g/l	The curve of removal compounds an increasing trend until 1.5 g/l TiO ₂ , which indicates that the rate is proportional to the total surface exposed.	39
Methylene blue (MB)	0.1 g TiO ₂ anatase	0.1 g	The photocatalytic activities decreased with the number of repeated uses except in the second use that showed highest photocatalytic activities.	40
Benzoic acid, phenol, and salicylic acid	TiO ₂ -coated (sol-gel)	3.14 cm ²	The relevant dynamics of desorption in the photodegradation of benzoic acid are $k=0.004 \text{ h}^{-1}$ (pH 9), $k=0.17 \text{ h}^{-1}$ (pH 7), and $k=0.10 \text{ h}^{-1}$ (pH 5).	41

TABLE II. (Continued.)

Target of compound	Photocatalyst	Using catalyst loading	Result	Reference
P-nitrosodimethyl-aniline	TiO ₂ , powder	0.3 g/l	Due to the stabilization by the resonance with the subsurface oxygen, there is some bond character between the adsorbed OH.	42
RY17, RB4, and RR2	TiO ₂	100–600 mg/100 ml	Beyond 300 mg of TiO ₂ , degradation increases in the case of RR2 and RB4 dyes up to 500 mg, and in case of RY17, degradation was constant with increase of TiO ₂ loading.	43
Methyl orange	Potassium peroxydisulfate	100–500 mg/l	The decolorization of MO increases with the increasing of the dosage of catalyst. When the catalyst is 5 g/l, decolorization of MO is up to 100%.	44
DBS (ZnO), KS (ZnO), DBS (TiO ₂), BS (TiO ₂)	TiO ₂	100 mg	The adsorption of PSS over TiO ₂ or ZnO particles is one of important factors to form SO ₄ ²⁻ ion.	45
Nylon simulated dyestuff effluent	TiO ₂	0.5 g/l TiO ₂ and 0.056 g/l Fe ⁺³	The dark adsorption of TiO ₂ surface led to a decrease of less than 15% of its concentration.	46
Rhodamine B (RB)	EDTA/TiO ₂ /O ₂ [·] , EDTA/TiO ₂ /N ₂ , TiO ₂ /O ₂ [·]	1 × 10 ⁻⁵ M	In the system studied, RB can only slightly be adsorbed on the TiO surface, so it cannot act as the main scavenger and become RB.	47
4-hydroxybenzoic acid and benzamide	TiO ₂	0.2–2 g/l	4-hbz proves to be a stronger competitor than Bz.	48

B. Modified catalysts

The base of heterogeneous photocatalysis is the combination of a semiconductor such as metal oxides (TiO_2 , ZnO , and Fe_2O_3) and metal sulfides (CdS and ZnS) as the photocatalysts with UV light.^{24,31,49}

C. Metal semiconductor modification

Various chalcogenides (oxides and sulfides) have been used: TiO_2 , ZnO , CeO_2 , CdS , ZnS , etc. In addition, anatase is the most active allotropic form among the various ones available, either natural (rutile and brookite) or artificial ($\text{TiO}_2\text{-B}$, $\text{TiO}_2\text{-H}$). Anatase is thermodynamically less stable than rutile, but its formation is kinetically favored at lower temperature ($<600^\circ\text{C}$).²⁸ Loading of Pt is optimum to achieve the maximum photocatalytic rate, affecting the distribution of electrons in the system. It is observed that, upon increasing (W^{6+}) concentration, the decolorization rate initially increases,⁵⁰ Co (III) ions work as electrons scavengers which may react with the superoxide species. The efficiency of the 2-CP photodegradation was 93.4% and 96.4% at pH of 9 and 12, respectively.⁵¹ The optimum loading of WO_3 or MoO_3 on TiO_2 was determined by measuring the activity of various WO_3/TiO_2 and $\text{MoO}_3/\text{TiO}_2$ samples³² and observed that Fe^{3+} -doping improves the photocatalytic activity of TiO_2 .⁵²

D. Composite semiconductors and surface sensitization

Coupled semiconductors are used to increase the separation between charges and reduce the energy (increasing wavelength) necessary to excite the system, which shows CdSTiO_2 as an example. The energy from light ($\lambda < 497\text{ nm}$) is large enough to cause an electron to leave the CdS valence band and go over to the conduction band. The hole remains in the CdS while the electron is transferred to the TiO_2 conduction band. The separate charges are then free to undergo electron transfer with the species adsorbed on the surface.⁵³

IV. APPLICATIONS OF PHOTOCATALYSIS

In recent years, environmental clean-up techniques have been implemented in many fields such as drinking water treatment, industrial, and health applications.⁹

A. Photodegradation of organic compounds

The equation given below can be considered as the basic reaction for the degradation of organic compound ($\text{C}_n\text{H}_m\text{O}_z\text{Cl}_y$). It can be seen that the products of the reaction are innocuous species,⁷



The higher reaction efficiencies would be achieved as increasing the excitation photon energy in the wavelength region of 400–340 nm. Experimental results indicate that the initial rate of photodegradation increases with increase in catalyst dose up to an optimum loading.^{33,54–60} It has been used for the destruction of organic compounds such as alcohols, acids, phenolic, and chlorinated aromatics into harmless products. This was observed for the following substituents—Cl, NO_2 , CONH_2 , CO_2H , and OCH_3 . If an aliphatic chain is bound to the aromatic ring, the breaking of the bond is easy, as it was observed in the photocatalytic decomposition of 2, 4-D (2, 4-dichlorophenoxy-acetic acid) and tetrachlorvinphos (Z)-2-chloro-1 (2, 4, 5-trichlorophenyl) ethenyl-dimethyl-phosphate and phenitrothion. Most of the pollutants which are in the nonexhaustive list, given in Table III, disappear following apparent first-order kinetics.^{28,34–36,61–63}

TABLE III. List of aqueous organic pollutants mineralized by photocatalysis.

Class of organics	Examples	Reference
Aldehydes	Acetaldehyde, formaldehyde	11 and 28
Alkanes	Methane, isobutane, pentane, heptane, cyclohexane, paraffins	
Aliphatic alcohols	Methanol, ethanol, propanol, glucose	
Aliphatic carboxylic acids	Formic, ethanoic, propanoic, oxalic, butyric, malic acids	
Alkenes	Propene, cyclohexene	
Haloalkenes	1,2-dichloroethylene, 1,1,2-trichloroethylene	
Aromatics	Benzene, naphthalene	
Haloalkanes	mono-, di-, tri-, and tetrachloromethane, tribromoethane, 1,1,1-trifluoro-2,2,2 trichloroethane	
Haloaromatics	Chlorobenzene, 1,2-dichlorobenzene	
Phenolic compounds	Phenol, hydroquinone, catechol, methylcatechol, resorcinol, <i>O</i> -, <i>M</i> -, <i>P</i> -cresol, nitrophenols	
Halophenols	2-, 3-, 4-chlorophenol, pentachlorophenol, 4-fluorophenol	
Aromatic carboxylic acids	Benzoic, 4-aminobenzoic, phthalic, salicylic, <i>M</i> - and <i>P</i> -hydroxybenzoic, chlorohydroxybenzoic and chlorobenzoic acids	
Carboxylic acids	Phenoxy acetic acid, 2,4,5-phenoxyacetic acid, oxalic acid monochloro-acetic acid	
Chlorophenols	2-chlorophenol, 4-chlorophenol, 2,4-dichlorophenol, 4-fluorophenol	
Dyes	Rhodamine B, methylene blue, methyl orange, fluorescein, acid orange 8 and acid red1, chrysoidine Y, acridine orange and ethidium bromide, indigo carmine, Chicago sky blue, mixed dye (mixture of the four dyes)	
Ethers	Methyl <i>tert</i> -butyl ether (MBTE), mixture of 4-chlorophenol, 2,4-dichlorophenol, 2,4,6-trichlorophenol, and pentachlorophenol	
Herbicides and fungicides	Atrazine, prometon, propetryne, bentazon, 2-4 D, monuron, isoproturon and fenamidone	
Perfluoroaliphatics	Trifluoroacetic acid, sulfonic acid of nonafluorobutane and heptadecafluorooctane	
Pesticides	DDT, parathion, lindane, tetrachlorvinphos, phenitrothion	
Surfactants	Sodium dodecylsulphate, polyethylene glycol, sodium dodecyl benzene sulphonate, trimethyl phosphate	

B. Effects of light intensity band gap and wavelength

For the study on the effect of light intensity on the photocatalysis process and kinetics at low light, (0–20 mW/cm²), the rate would increase linearly with increasing light intensity. It has been earlier studied that the heterogeneous photocatalytic oxidation processes can be used in the presence of light for removing coloring material from dye effluent. It is evident that the percentage of decolorization and photodegradation increase with the increase in irradiation time indicates that (Fig. 2) the wavelength of radiation required activating the catalysts.^{4,64–67} Table IV shows the band gaps and physical properties of some semiconductors used in photocatalysis.⁷ The minimum wavelength required to promote the excited state depends on the band-gap energy.⁶⁸ The electron excited state probability of an electronic transition is proportional to the square of the amplitude of the radiation field E_0 and the square of the transition dipole moment $|\mu_{if}|$,^{69,70}

$$P \propto E_0^2 |\mu_{if}|^2. \quad (7)$$

The amplitude of the radiation field E_0 can be controlled by varying the light intensity. At low light intensities, the degradation rate increases linearly;²³ at midrange light intensities, the rate is de-

TABLE IV. Band-gap energies of semiconductors used for photocatalytic processes.

Photocatalyst	Band-gap energy (eV)	Reference
Si	1.1	7 and 53
WSe ₂	1.2	
WO ₃	2.8	
α -Fe ₂ O ₃	2.2	
V ₂ O ₅	2.7	
SiC	3.0	
BaTiO ₃	3.3	
CdO	2.1	
CdS	2.4	
CdSe	1.7	
Fe ₂ O ₃	3.1	
TiO ₂ rutile	3.02	
TiO ₂ anatase	3.23	
Sr TiO ₃	3.4	
SnO ₂	3.5	
GaP	2.3	
GaAs	1.4	
SrTiO ₃	3.4	
TiO ₂	3.0	
ZnS	3.7	
ZnO	3.2	

pendent on the square root of intensity; and at high intensities the degradation rate is independent of intensity. For example, TiO₂ anatase, a stable photocatalyst with large band-gap energy (3.2 eV), is active only in the ultraviolet region of the solar spectrum. Although the cadmium sulfide (CdS) semiconductor has a smaller band gap (2.4 eV) and works in the visible range, it is not sufficiently positive to act as an acceptor. This causes the photocatalyst to decompose with hole formation.²⁷ Table V shows that the variations of the reaction rate as a function of the wavelength follow the absorption spectrum of the catalyst, with a threshold corresponding to its band-gap energy. TiO₂ requires $\lambda \leq 400$ nm, i.e., near-UV wavelength (UV-A).²⁸ Tables VI summarizes the study of degradation rate with light intensity by adjusting the distance between the UV lamp and reactors.³⁷

C. Adsorption under dark condition

The role of a catalyst is to accelerate the rate of the reaction without being consumed in it. The photolytic reactions carried out in the absence of a photocatalyst exhibit very low efficiency as compared to the reactions in the presence of a catalyst.⁷¹ The optimal experimental conditions in Fig. 3 show the behavior of the chemical oxygen demand (COD) reduction for different catalyst concentrations and it is also seen that no degradation occurred in the dark condition. It was found that the degradation rate of catalyst increased linearly with increasing light intensity up to a certain limit, where it reached a plateau indicating high recombination reactions.²⁷ After the first test (no UV activation-1), the reactor appeared blue colored due to methylene blue (MB) adsorption. The blue color of the reactor was stronger at the end of the second test (no UV activation-2), thus less sites were available for MB adsorption in the third test (after UV activation).³⁵

D. Effect of pH

The influence of pH, the surface charge of the semiconductor affects the interfacial electron transfer and therefore the photoredox process. The influence of the pH of surface charge of the semiconductor affects the interfacial electron transfer and therefore the photoredox process. At

TABLE V. Different sources for hydroxyl generation in advanced oxidation process.

Method		Key reaction		Light necessary (nm)	Reference
UV/H ₂ O ₂	$\text{H}_2\text{O}_2 + \text{h}\nu \rightarrow 2\text{OH}\cdot$			$\lambda < 310$	2
UV/O ₃	$\text{O}_3 + \text{h}\nu \rightarrow \text{O}_2 + \text{O}(1\text{D})$	$\text{O}(1\text{D}) + \text{H}_2\text{O} \rightarrow 2\text{OH}\cdot$		$\lambda < 310$	
UV/H ₂ O ₂ /O ₃	$\text{O}_3 + \text{H}_2\text{O}_2 + \text{h}\nu \rightarrow \text{O}_2 + \text{OH}\cdot + \text{OH}_2\cdot$			$\lambda < 310$	
UV/TiO ₂	$\text{TiO}_2 + \text{h}\nu \rightarrow \text{TiO}_2(\text{e}^- + \text{h}^+)$	$\text{TiO}_2\text{h}^+ + \text{OH}\cdot_{\text{ad}} \rightarrow \text{TiO}_2 + \text{OH}\cdot_{\text{ad}}$		$\lambda < 380$	
	$\text{IO}_4^- + \text{h}\nu \rightarrow \text{IO}_3^- + \text{O}\cdot^-$	$\text{O}\cdot^- + \text{H}^+ \rightarrow \cdot\text{OH}$	$\cdot\text{OH} + \text{IO}_4^- \rightarrow \text{OH}^- + \text{IO}_4\cdot$	$\lambda < 380$	
UV/H ₂ O ₂ /TiO ₂	$\text{TiO}_2 + \text{h}\nu \rightarrow \text{TiO}_2(\text{e}^- + \text{h}^+)$	$\text{TiO}_2\text{h}^+ + \text{OH}\cdot_{\text{ad}} \rightarrow \text{TiO}_2 + \text{OH}\cdot_{\text{ad}}$	$\text{H}_2\text{O}_2 + \text{e}^- \rightarrow \text{OH}\cdot + \text{OH}^-$	$\lambda < 380$	
UV/S ₂ O ₈ ²⁻ /TiO ₂	$\text{TiO}_2 + \text{h}\nu \rightarrow \text{TiO}_2(\text{e}^- + \text{h}^+)$	$\text{TiO}_2\text{h}^+ + \text{OH}\cdot_{\text{ad}} \rightarrow \text{TiO}_2 + \text{OH}\cdot_{\text{ad}}$	$\text{S}_2\text{O}_8^{2-} + \text{e}^- \rightarrow \text{SO}_4^{\cdot-} + \text{SO}_4^{2-}$	$\lambda < 380$	
H ₂ O ₂ /Fe ²⁺ (Fenton-reaction)	$\text{H}_2\text{O}_2 + \text{Fe}^{2+} \rightarrow \text{Fe}^{3+} + \text{OH}\cdot + \text{OH}^-$...	
UV/H ₂ O ₂ /Fe (photo-Fenton reaction)	$\text{H}_2\text{O}_2 + \text{Fe}^{2+} \rightarrow \text{Fe}^{3+} + \text{OH}\cdot + \text{OH}^-$	$\text{Fe}^{3+} + \text{H}_2\text{O} + \text{h}\nu \rightarrow \text{Fe}^{2+} + \text{H}^+ + \text{OH}\cdot$		$\lambda < 580$	

TABLE VI. The effects of light/wavelength on photocatalytic processes.

Target of compound	Light source	Intensity	Irradiation time	Result	Reference
C.I. reactive red 198	500 W Hg lamp (254 nm)	300 mW/cm ²	10 (min) at pH 4, 0–30 (min) at pH 7, 60 (min) at pH 10	The primary decolorization pathway involves hydroxyl radicals and that direct oxidation by photogenerated holes is significant in the UV/TiO ₂ system.	3
Fast green FCF (1), patent blue VF (2)	125 W Hg lamp		0–80 (min)	Spectra at 625 nm after 33% with TiO ₂ (1 g/l) patent blue VF (2, 0.125 mM, 250 ml). Spectra at 638 nm after 64% dilution.	4
Acridine orange and 3,6-diaminoacridine	15 W UV tubes (365 nm), two sides		0–24 (h)	The UV-visible spectra during the process of the AO dye are illustrated. About 99.7% of the dye was degraded after irradiation for 24 h.	5
Azo dye acid red 114	32 W (UVC) mercury lamp		0–200 (min)	Mixed photocatalyst (10 wt % TiO ₂ /CP) and UV irradiation, 92.9% of dye was degraded at the irradiation time of 2.5 h.	8
Azo dye [AR27]	30 W mercury lamp (UV-C, 254 nm)	1–8.6 W/m ² .	0–0.3 kap min ⁻¹ .	The value of 0.5 for UV-light intensity order in degradation in the UV/TiO ₂ and UV/ZnO processes at higher UV-light intensities.	13
Direct yellow 12 dye	8–40 W UV lamps	25–50 W/m ²	0–120 (min)	The rate of degradation increases with increase in UV intensity as more radiations fall on the catalyst.	26
Portion H-cell dyes	H ₂ O ₂ /UV 9 W lamp (254 nm)		0–50 (min)	Between 10 and 500 mg/l at pH 4, 7, and 10, decolorization rates decrease as dye increases, specially above 100 mg/l.	29
DNS DA, ANSDA, and DAS DA	15 W UV lamp (300–450 nm)		TiO ₂ /UV, 2.5 (h) and Fe ²⁺ /H ₂ O ₂ /UV, 25 (min)	The time required for 90% TOC removal was 10, 12, and 16 h in TiO ₂ /UV process whereas it was 180, 150, and 90 min in Fe ²⁺ /H ₂ O ₂ /UV process, respectively.	30
Chrysoidine Y (1)	125 W mercury lamp		0–120 (min)	To obtain a high degradation rate, this is essential for any practical application of photocatalytic oxidation processes.	31
Methyl orange	500 W Hg lamp (365 nm), in center		0–21 (min)	There was no degradation in the absence of irradiation.	52
Chlorobenzene	125 W UV lamp, in bottom (365 nm)		0–60 (min)	The degree of degradation that is reached within 1 h using UV radiation requires 2 h of concentrated solar radiation.	63
Naphthalene	HPK 125 W mercury lamp		Below 10 ¹⁶ photons/s	The increase in the photonic flux does not induce a proportional increase in the degradation rate.	34

TABLE VI. (Continued.)

Target of compound	Light source	Intensity	Irradiation time	Result	Reference
Methylene blue (MB)	UV lamp (335 nm), in vertically	3.0 and 1.1 mW/cm ²	0–500 time (min)	UV radiation is useful to both mineralize organic compounds adsorbed on the catalyst and to activate the catalyst.	35
Methylene blue (MB)	75 W Hg lamp (λ_{\max} = 360 nm)	0.98–7.2 mW/cm ²	0–120 (min)	Photons entering the reaction produce the quantity of holes (h ⁺) which ultimately lead to oxidative photodegradation.	36
4BS azo dye	250 W Hg lamp (300–410 nm)	1 $\times 10^3$ μ W/mm ²	0–30.0 (min)	With an increased catalyst dosage of enough power, the control step changes to the factor of a no catalyst dosage.	37
Winery wastewater	Hg UV lamp (310–435 nm)		0–60 (h)	To confirm this notion that light shielding is responsible for decreased reaction rates in the presence of TiO ₂ catalyst.	38
Pesticide pyridaben in CTAB	350W Hg UV lamps, inside	7.8 mW/cm ²	0–150 (min)	Study of homogeneous photo-oxidation, direct photolysis of H ₂ O ₂ by UV light can generate •OH radicals directly.	39
Methylene blue (MB)	UV light (5 tubes, 20 W)	...	1–5 (h)	The rubber surface was covered with trace of impurities during the preparation and was destroyed.	40
Benzoic acid, phenol, and salicylic acid	TiO ₂ -coated (sol-gel)		0–24 (h)	Do not correlate with the extent of initial adsorption/desorption of the substrate on the TiO ₂ .	41
P-nitrosodimethyl-aniline	100 W Hg lamp (λ > 330 nm)		0–25 (min)	The isobestic point at 380 nm implicates a quantitative balance between the disappearance of P and formation of I.	42
RY17, RB 4, and RR 2	6 \times 8 W Hg arc lamp (254 nm)		0–14 (h)	The difference in the rate of degradation is attributed to difference in the input energy.	43
Methyl orange	30 W lamp (254 nm)		0–100 (min)	Such as the reaction rate constants (Kobs), half-life (t _{0.5}) and interrelated coefficients (R2) of the lines.	44
DBS (ZnO), KS (ZnO), DBS, BS (TiO ₂)	100 W Hg lamp		0 to 8 (h)	The aqueous organic/TiO ₂ dispersions become acidic immediately and TiO ₂ surface is charged positively upon UV irradiation lb, lc.	45
Nylon simulated dyestuff effluent	UV reflective (300–400 nm)	10 and 35 W m ⁻²	1 (h)	In this case the photo-Fenton reagent is more effective in comparison to the TiO ₂ /oxidant system.	46

TABLE VI. (Continued.)

Target of compound	Light source	Intensity	Irradiation time	Result	Reference
Rhodamine B (RB)	100 W UV light, Hg lamp ($\lambda > 330$ nm)			The adsorbed H O or OHy with the holes under UV light 2 irradiation is involved in the photo-oxidation on the TiO surface.	47

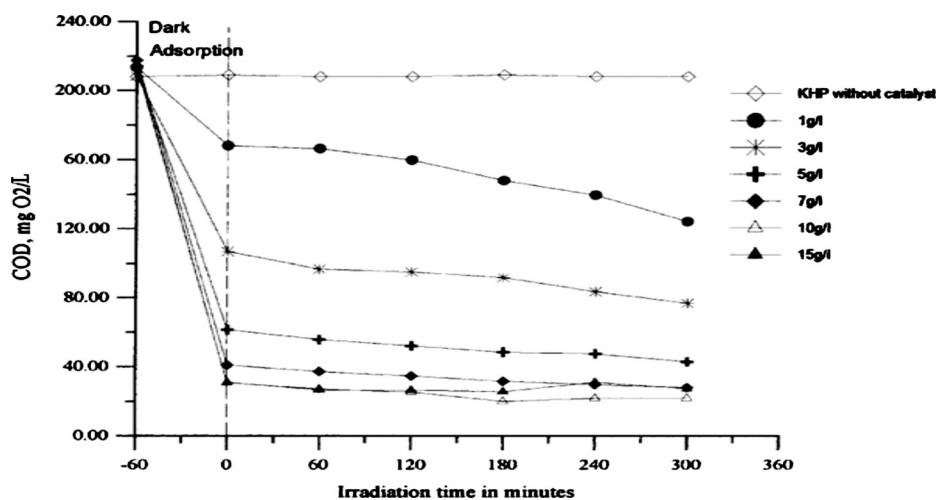


FIG. 3. The different irradiation times for the solution at different Hombikat UV 100 concentrations.

higher pH values, the formation of active $\cdot\text{OH}$ species is favored, not only because of improved transfer of holes to the adsorbed hydroxyls, but also due to electrostatic attractive effects operating between the negatively charged TiO_2 particles and the cationic dye.⁵ As it was studied that acidic conditions (with pH values less than 2) did not favor the photocatalytic oxidation, as the pH value increased further, the removal percent decreased rapidly.³⁸ Table VII observed that the pH is an important factor significantly affecting adsorption and the initial rate of degradation.⁷³ The degradation rates at the different pH values were calculated from the measured COD.²⁷ A plot of the degradation rate versus pH is illustrated in Fig. 4.

E. Effect of initial concentration

Most authors agreed that the expression for the rate of photomineralization of organic substrates with irradiated TiO_2 follows the Langmuir–Hinshelwood (LH) law for the same saturation-type kinetic behavior in any of four possible situations: (i) the reaction takes place between two adsorbed substances, (ii) the reaction occurs between a radical in the solution and the adsorbed substrate, (iii) the reaction takes place between the radical linked to the surface and the substrate in the solution, and (iv) the reaction occurs with both species in solution. It is important both from a mechanistic and application point of view to study the dependence of substrate concentration on the photocatalytic reaction rate of the pollutants.⁴ The presumed reason is that when the initial concentration of dye is increased, more and more dye molecules are adsorbed on the surface of TiO_2 .⁸ The degradation rate at this concentration reached more than double its value in comparison to the 1 g/l concentration. Figure 5 shows that the further increase of the TiO_2 concentration produced no significant improvement in the degradation rate.²⁷ Table VIII summarizes studies that have obtained similar experimental findings for UV/ TiO_2 -based systems^{74–80} and this phenomenon has three possible explanations.

- (i) First, a significant quantity of UV light may be absorbed by the highly concentrated dye molecules rather than by the TiO_2 particles, thereby reducing decolorization efficiency. The dye therefore has a UV-screening effect, fewer photons reach the TiO_2 surface as dye concentration increases, slowing the formation of $\text{OH}\cdot$ radicals.
- (ii) Second, as the initial concentration of dye increased, the TiO_2 surfaces adsorbed additional dye molecules, which inhibited direct contact between the dye molecules and photogenerated holes and which also suppressed the generation of hydroxyl radicals at the TiO_2 surface as dye molecules covered active surface sites.
- (iii) Third, the increased amounts of dye and reaction intermediates competed with both hydroxyl radicals and active reaction sites at the TiO_2 surface. Hence, the fraction of hydroxyl

TABLE VII. Effects of the pH.

Target of compound	pH studied	Result	Reference
C.I. reactive red 198	pH 4, 7, and 10	The decolorization of UV/TiO ₂ at pH 4, 7, and 10 was 98%, 57%, and 35%, that of UV/TiO ₂ /Na ₂ S ₂ O ₈ was 99%, 78%, and 48%, respectively, and that of UV/TiO ₂ /H ₂ O ₂ was 99%, 84%, and 51%, respectively.	3
Fast green FCF (1) and patent blue VF (2)	FCF (1) pH 3, 4.4, 9, 11 and patent value VF (2), pH 3, 5.4, 9, and 11	The efficiency of degradation rate for the decomposition of dye 1 was found to increase with an increase from pH 3 to 4.4, a further increase in pH leads to a decrease in the rate. On the other hand, in the case of dye derivative 2, the degradation rate increases with the increase in pH from 3 to 11, the highest efficiency was observed.	4
Acridine orange and 3,6-diaminoacridine	pH 3, 6, 9,	Under alkaline conditions, the TiO ₂ surface carries a weak negative charge, while AO is primarily positively charged which will facilitate adsorption and promote photocatalytic degradation.	5
Azo dye acid red 114	pH 2, 4, 6, 8, 10, 12	At different pH shows, the best results were obtained in acidic solution (pH=2, X=100%).	8
Diazo direct yellow 12 (Chrysophenine G)	pH 4.5, 6.8, 8.0, 11.00	In highly acidic medium, rate of degradation is high and decreases, as the pH of the solution is increased up to 11.	26
Portion H-ell dyes	pH 3, 6, 9	In acidic pH, Ceq reaction progresses and the dye concentration in the solution further decreases, the decolorization rates quickly slow down when compared to the corresponding rates in neutral and alkaline pH.	29
DNSDA, ANSDA, and DASDA	pH 2.0, 3.0, 4.0, 5.0, 6.0, 7.0, and 8.0	pH between 3.0 and 4.0 was favorable for removal of all the test compounds. Previous studies on Fe ²⁺ /H ₂ O ₂ /UV process also reported that the optimal pH for a Fenton reaction was 3.0.	30
Chrysoidine Y (1)	pH 3.5, 5, 7, and 9	The degradation rate for the mineralization and decomposition of dye was found to be lower at lower pH values, which increases with increase in reaction pH.	31

TABLE VII. (Continued.)

Target of compound	pH studied	Result	Reference
Chlorobenzene	pH 7.0, 9.8, 8.2, 3.3, 5.0	At pH 8.2, the degradation of chlorobenzene was 98% and that of TOC was 97%. In the case of pH 9.8, the degradation of chlorobenzene was 98% and of TOC was 97.5%.	63
Naphthalene	pH 2, 4, 6, 8, 10, 12, 14	Higher adsorption at higher pH, which is assumed to be linked to double layer modification at the surface.	34
Methylene blue (MB)	pH 4, UV on (pH 7), pH 9	The MB removal was completely inhibited at pH 4. Conversely, at pH 9, an almost instantaneous decrease in UV664 peak indicated removal up to 80% in the first 10 min.	35
Methylene blue (MB)	pH 1.85, 2.98, 3.85, 5.32	Wavelength shifts at pH=1.85 are nearly negligible and the degradation rate was slowest, greater wavelength changes were observed at other pHs, with the greater change occurring at pH=3.85.	36
4BS azo dye	pH 3, 5, 7, and 11	The minimum decolorization is around pH 9. With the decrease of pH of the dye solution from 9 to 1, the increase from 82.5% to 98%, with an increase of pH from 9 to 12, the increase of decolorization is from 82.5% to 95%.	37
Winery wastewater	pH 3, 6, 9, 12	It indicates that increasing the pH from 4 promoted the degradation rate but it reaches a maximum rate at pH 6.5.	38
Cetyltrimethyl ammonium bromide	pH 3.00, 5.72, 6.72, 8.64, 9.40, and 10.87	The pH has little effect on the disappearing rate between pH 3.0 and 6.0, and there existed a gradual increase with the increase of pH from 6.0 to 8.0. The most remarkable increase occurred when pH increased to 10.83.	39
Methylene blue (MB)	pH 3, 5, 6.86, 8	The order of activities is pH 8 > pH 6.86 > pH 5 > pH 3.	40
Benzoic acid, phenol, and salicylic acid	pH 7, 5, 9	The faster degradation thus takes place at pH 9 for salicylic acid.	41

TABLE VII. (Continued.)

Target of compound	pH studied	Result	Reference
P-nitrosodimethylaniline	pH 1.8, 3.4, 3.9, 6.6, 9.5	Redox potentials of $h\nu$ and e^- play a dominant role in determining the reactivity of photocatalytic bleaching of P.	42
(RY17), [RB4], and (RR2)	pH 3, 4, 5, 6, 7, 8, 9, 10, 11, 12, 13	At optimum concentration of dyes in both acidic and alkaline pH, it seems to decrease the percentage degradation of the dyes.	43
4-hydroxybenzoic acid (4-HBz) and benzamide (Bz)	Bz pH 3.4, 5.7, 7.8, 9.0 and 4-HBz pH 4.2, 5, 5.5, 6.2, 7, 9.4	The pH has a strong effect at pH levels lower than the pH_{zpc} of TiO_2 , the higher the adsorption, the higher the degradation, and at higher pH values, the change of surface charge of TiO_2 leads to a supplementary repulsive phenomenon lowering the degradation of the ionic state.	48
Branched C4 and C5 carboxylic acids	pH 3.7, 3.8	The pH of all the acid solutions remained around 3.7–3.8. Branching had little impact, if any, on dark adsorption of C4 and C5 aliphatic carboxylic acids, and consequently played no role in the adsorption process.	72
Photoreduction of a metal ion Ag^+	pH 4, 6	The pH behavior of the photodeposition is different as evidenced by the waveforms seen at pH 6 versus pH 4. At pH 6, the mass changes again, fluctuated until about 40 min of irradiation and then stabilized.	71

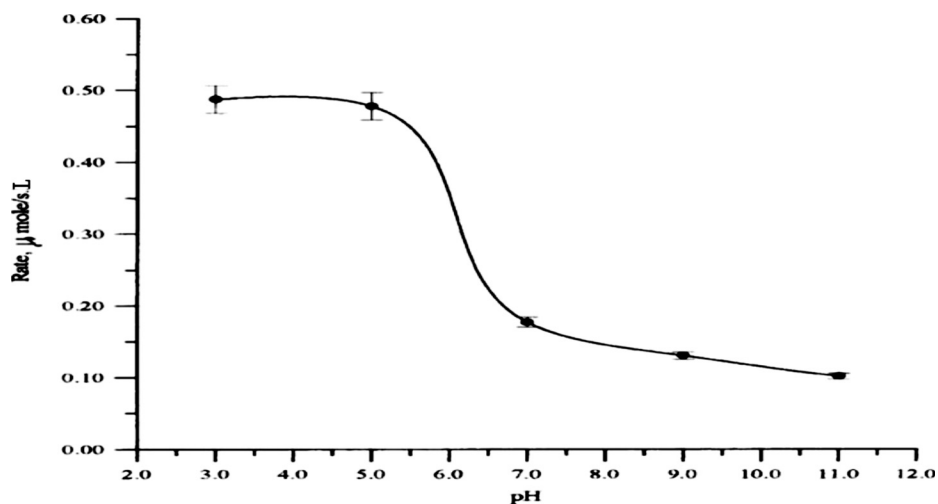


FIG. 4. The degradation rate of the solution at different pH levels.

radicals that attacked the dye molecules and its reaction intermediates declined as the dye concentration increased.³

In contrast, considering the Beer–Lambert law, as the initial dye concentration increased, the path length of the photons entering the solution decreased, resulting in lower photon absorption on catalyst particles and accordingly lower photodegradation rate.⁵

F. Effects of ions

The effect of the various anions on the photocatalytic degradation using UV radiation has also been studied. It was observed to be negligible and 98%–99.5% degradation in chlorobenzene and total organic carbon (TOC) was found within 1 h. This behavior was similar to that using concentrated solar radiation.⁶³ The percentage ionic characters of the MO bond for some of the semiconductors are TiO_2^- 59.5, BaTiO_3^- 70.8, and Fe_2O_3^- 47.3.⁸¹

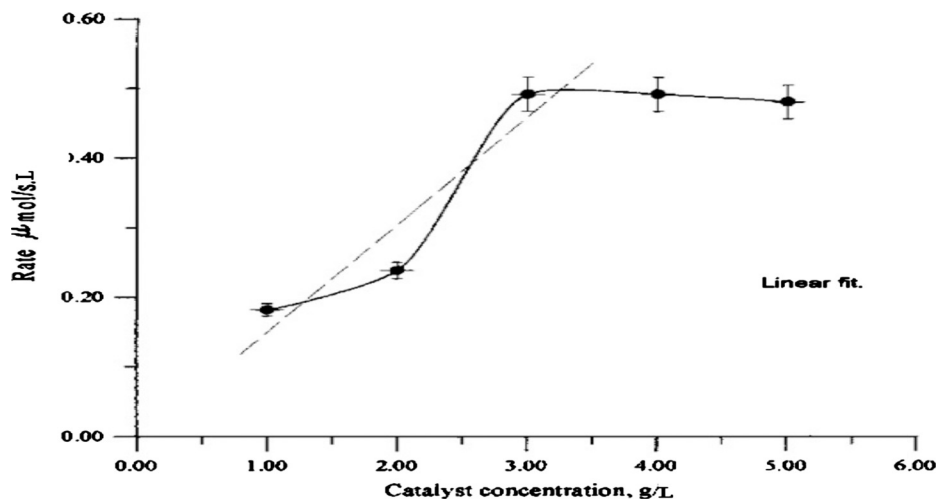


FIG. 5. Degradation rate at different catalyst concentrations.

TABLE VIII. The influence of initial concentration and their effects.

Target of compound	Initial concentration	Result	Reference
C.I. reactive red 198	10–80 ppm at pH 7 in the UV/TiO ₂ system	Increased amounts of dye and reaction intermediates competed with both hydroxyl radicals and active reaction sites at the TiO ₂ surface, dye concentration increased.	3
Fast green FCF (1) and patent blue VF (2)	0.031, 0.064, 0.093, and 0.125 mM (dye 1) and 0.064, 0.093, 0.125, and 0.18 Mm (dye2).	The degradation rate of the dye derivatives 1 and 2 respectively indicates that the rate decreases with the increase in the substrate concentration.	4
Acridine orange and 3,6-diamino-acridine	(Stock solutions 1 g l ⁻¹) 0.05, 0.15, 0.25g/l	The concentration increased, the path length of the photons entering the decreased, resulting in lower photon absorption on catalyst particles and, consequently, lower degradation rate.	5
Azo dye acid red 114	20–80 ppm	The presumed reason is that the initial concentration of dye is increased, more and more dye molecules are adsorbed on the surface of TiO ₂ .	8
Azo dye (AR27)	5–45 mg l ⁻¹ .	The molar extinction of the dye is high, so that a rise in its concentration induces an inner filter effect, and hence the solution becomes more and more impermeable to UV radiation.	13
Diazo direct yellow 12	100–500 ppm	Initial concentration increases, more and more organic substances are adsorbed on the surface of TiO ₂ , but the intensity of light and illumination time are constant.	26
Degradation of portion H-ell dyes	75, 100, 200 mg/l	The decolorization of the portion H-ell dilute solutions examined strongly depends on the system parameters in all five AOPs studied	29
DNSDA, ANSDA, and DASDA	0.05–0.20 mg/l	TiO ₂ /UV—the test compounds disappeared very fast at lower concentrations and as the concentration increased the rates of decomposition were decreased. Fe ²⁺ /H ₂ O ₂ /UV—it could be seen that the rate constants were decreased with an increase in the initial concentration.	30

TABLE VIII. (Continued.)

Target of compound	Initial concentration	Result	Reference
Chrysoidine Y (1)	0.125, 0.25, 0.35, 0.5, 0.75, and 1 mM	It is interesting to note that the degradation rate increases with the increase in substrate concentration from 0.125–0.75 to 1 mM lead to a decrease in degradation rate of the dye.	31
Chlorobenzene	500 mg/dm ³	Initial pH of 3.3, 5 and 8.2, chlorobenzene and TOC removals was 98%, 99%, and 98% respectively with in 1 h.	63
Naphthalene	20–80 μ mol/l	The reaction rate increases linearly with concentration up to 40 μ mol/l.	34
Methylene blue (MB)	Added 20 mg of MB to 3 L (18 μ M/l)	Changes in MB concentration (UV664 peak area) at pH 7 amounted to 24% and 48% after 1 and 3 h, respectively. At pH 9, removal efficiency reached 80% after 10 min.	35
Methylene blue (MB)	0.01–0.10 mM	MB degrades at relatively high initial concentrations (0.3 mM) in UV-illuminated aqueous TiO ₂ dispersions by first-order kinetics ($k=1.5 \pm 0.1 \times 10^{-2} \text{ min}^{-1}$).	36
4BS azo dye	0–45 $\times 10^{-3}$ /g/l.	UV light absorbed by solution increased, that means less photons can reach the photocatalyst surface and hydroxyl radicals reduce, so the decolorization decreases.	37
Winery wastewater	38.5 l	The TOC measurement gives a more realistic of total organic carbon than either biochemical oxygen demand, assimilable organic carbon, or COD measurements.	38
Cetyltrimethyl ammonium bromide	CTAB concentration 2.7434×10^{-3} M	Amount of pyridaben dissolved helps to obtain an appropriate kinetics and avoid inaccuracy in the determination of the initial rate constant, but not too much to retard the reaction.	39
Methylene blue (MB)	60 ml of MB solution (2.5×10^{-5} M) at given irradiation time intervals (every 1 h), 4 ml of MB solution sample was collected.	For the case of highest photocatalytic activities, this may result from the fact that the rubber surface was covered with trace of impurities during the preparation and was destroyed during the first photodegradation along with MB molecules in solution.	40

TABLE VIII. (Continued.)

Target of compound	Initial concentration	Result	Reference
Benzoic acid, phenol, and salicylic acid	0.0025–0.0125 mM	The mass of benzoic acid adsorbed on the TiO ₂ particles was about the same at pHs 5 and 7 {264 ng [0.69 nmol/cm ²] (pH 5), 247 ng [0.64 nmol/cm ²] (pH 7)} increasing to 520 ng [1.36 nmol/cm ²] in alkaline media (pH 9) for an initial concentration of 0.01 mM in substrate	41
RY17, RB4, and RR2	8×10^{-4} to 1.2×10^{-3} M (RY17), 4.16×10^{-4} to 1.25×10^{-3} M in (RR2), 1×10^{-4} to 5×10^{-4} M (RB4)	The initial concentration of the dye increases, the path length of photons entering the solution decreases, and in low concentration, the reverse effect is observed, thereby increasing the number of photon absorption by the catalyst in lower concentration.	43
Methyl orange	6, 10–120 mg/l	The initial photocatalytic decolorization rate (r^0) is observed to be a function of the initial concentration (C^0).	44
DBS, KS (ZnO), DBS (TiO ₂), BS (TiO ₂)	0.1 mM, 20.6 mg/l	The photodecomposition of SDS and DS are small with ZnO, the TiO ₂ gave larger amounts of SO ₄ ²⁻ in the decomposition of SDS than in that of DS.	45
Nylon simulated dyestuff effluent (NSW)	0.1126 g/l	The decolorization of a BGT in the presence of the photo-Fenton reagent (0.056 g/l Fe ⁺³ /0.51 g/l H ₂ O ₂) showed that this process is faster in comparison to the TiO ₂ /H ₂ O ₂ system.	46
Rhodamine B (RB)	Initial 1×10^{-5} M.	Both holes in the valence band of semiconductors and hydroxyl radicals.	47
4-HBz and Bz	$[4\text{-HBz}]_4^1 0.1$ mmol/l and $[\text{Bz}]_4^1 0.2$ mmol/l	We divided by 2 the molar concentration of the acid (0.1 mmol l ⁻¹) compared to the Bz (0.2 mmol l ⁻¹) concentration to evaluate the influence of the 4-HBz concentration.	48

TABLE IX. The more positive the potential, the better the species is an oxidizing reagent.

Oxidizing reagent	Oxidation potential (V)	Reference
Fluorine	3.06	53
Hydroxide radical ($\bullet\text{OH}$)	2.80	
Ozone	2.07	
Hydrogen peroxide	1.77	
Chlorine dioxide	1.57	
Chlorine gas	1.36	
Oxygen	1.23	
Hypochlorite	0.94	
Iodine	0.54	
Superoxide radical ($\text{O}^{2-\bullet}$)	-0.33	

G. Effects on different oxidizing reagent

In recent years, research in new nonbiological methods has led to processes, which actually destroy these pollutants instead of simply extracting them from water. Irmak *et al.*⁸² showed that the use of TiO_2 , O_3 , H_2O_2 , and Fenton (a mixture of ferrous ion with H_2O_2) is more efficient in the photodegradation of organic pollutants in comparison to that of direct photolysis. Malato *et al.*² reported that the use of inorganic oxidants, such as H_2O_2 , ClO_3^- , BrO_3^- , and $\text{S}_2\text{O}_8^{2-}$, in TiO_2 system increased the quantum efficiencies.^{82,83} A group of oxidants utilized in this work is oxyhalogens, which have more than two oxygen atoms and one halogen atom (Cl, Br, or I) at the center of the molecule. The higher reactivity of $\text{TiO}_2/\text{IO}_4^-$ is due to the production of highly reactive intermediate radicals such as $\text{IO}_3\cdot$, $\bullet\text{OH}$, and $\text{IO}_4\cdot$ (Ref. 82), also assisted the degradation by free radical pathways.⁸⁴ Study of homogeneous photo-oxidation,⁸⁵ direct photolysis of H_2O_2 by UV light, can generate $\bullet\text{OH}$ radicals directly by homolytic cleavage of bonds into two hydroxyl groups.^{39,82,84} The addition of H_2O_2 to the heterogeneous system increases the concentration of OH radical, since it inhibits the electron hole recombination, according to equations (Tables I and V). However, at high concentration of H_2O_2 , it also acts as a scavenger. Various studies have demonstrated that reactive radical intermediates, generated from per sulfate ions reacting with photogenerated electrons, accelerate decolorization in the $\text{UV}/\text{TiO}_2/\text{S}_2\text{O}_8^{2-}$ system.³ The reaction mechanism in the presence of $\text{S}_2\text{O}_8^{2-}$ seems to be expressed by equations. Electron acceptors or oxidizing reagent (Table IX) are an important role in the photocatalytic degradation (Table X) such as H_2O_2 , potassium bromate, and ammonium persulfate, etc., added into the solution.⁴

H. Effects of flow rate

The effect of gas flow on photodegradation of wastewater makes it clear that the average reaction rate increases with increasing gas flow rate. The decreased gas-liquid interface and shortened residence time of oxygen retard the oxidation rate. de Lasa *et al.*⁸⁶ investigated that such measurements on dissolved oxygen should be carried out.³⁸ Yin *et al.*³⁷ study that at increased stirring speeds, the bulk solution much improved the mixing and transport to the catalyst surface.

I. Effects of temperature

The photocatalytic systems have been studied due to their ability to photosensitize the complete mineralization of a wide range of organic substrates at ambient temperatures and pressures, without the production of harmful byproducts.⁵⁴ Because of photonic activation, photocatalytic systems do not play a significant role in photochemical processes, thus not require heat and operate at room temperature. The decrease in temperature favors adsorption, which is a spontaneous exothermic phenomenon.^{2,53} As a consequence, the optimum temperature is generally between 20 and 80 °C.^{87,88}

TABLE X. The influence of effects of ions/electron acceptors/oxidizing reagents.

Target of compound	Anions	Result	Reference
C.I. reactive red 198	UV/TiO ₂ , UV/TiO ₂ /Na ₂ S ₂ O ₈ , and UV/TiO ₂ /H ₂ O ₂	Adding Cu ₂₊ suppressed the recombination of photogenerated electron/hole pairs and generated additional persulfate free radicals in the UV/TiO ₂ /Na ₂ S ₂ O ₈ system, thereby accelerating decolorization. The UV/TiO ₂ /H ₂ O ₂ /Cu system resembles the photo-Fenton-like process since the induced photo-Fenton-like reactions acted as an additional source of hydroxyl radicals.	3
Fast green FCF (1) and patent blue VF (2)	H ₂ O ₂ (10 mM), (NH ₄) ₂ S ₂ O ₈ (3 mM), and KBrO ₃ (3 mM)	It was observed that potassium bromate and ammonium persulfate had a beneficial effect on the degradation rate for the decomposition of the dye 1 in the presence of UV100, whereas in the case of dye 2, all the electron acceptors were found to enhance the rate markedly in the presence of P25.	4
Azo dye(AR27)	Oxygen concentration	1.8 ≤ [O ₂] ≤ 20 mg/l that the quantum efficiency of photoassisted oxidation of organic compounds in water by O ₂ on TiO ₂ surfaces can be limited by kinetics of the reduction of O ₂ .	13
Diazo direct yellow 12 (Chrysophenine G)	H ₂ O ₂	The addition of hydrogen peroxide to the heterogeneous system increases the concentration of OH radical, since it inhibits the electron hole recombination.	26
Portion H-ell dyes	Cl ⁻ , H ₂ PO ₄ ⁻ , HCO ₃ ⁻ , CO ₃ ²⁻ , SO ₄ ²⁻ , and NO ₃ ⁻	All anions examined affect the decolorization rate adversely but to a varying degree. The trend is somewhat different at a lower anion concentration (0.01 M) when compared to a higher one (0.1 M).	29
(DNSDA), (ANSDA), and (DASDA)	H ₂ O ₂	Thus, the H ₂ O ₂ concentration was optimized between 8 mM and 15 for removal of 0.1 mM of the test compounds from water.	30
Chrysoidine Y (1)	ZnO (0.25 mM), V=250 ml, (1 GI ⁻¹), electron acceptors: KBrO ₃ (3 mM) and H ₂ O ₂ (10 mM)	Therefore, we have studied the effect of electron acceptors such as hydrogen peroxide and potassium bromate on the photocatalytic degradation of the dye. The degradation rate for the TOC depletion and decomposition of dye in the presence of two selected electron acceptors.	31

TABLE X. (Continued.)

Target of compound	Anions	Result	Reference
Chlorobenzene	NaCl, Na ₂ SO ₄ , NaNO ₃ , NaHCO ₃ , Na ₂ CO ₃	The adverse effect of carbonate and bicarbonate on the adsorption of chlorobenzene on TiO ₂ was more than the effect of chloride, sulfate, and nitrate.	63
Naphthalene	Na ₂ CO ₃ , NaHCO ₃ , and NaCl	Such as pH can moderate inhibition at low concentrations sodium chloride (0.6 mol/l) and sodium hydrogen carbonate (0.03 mol/l) to determine the rate of degradation in near-seawater conditions (hydrogen carbonate ions make pH raise to 8.4). Sodium chloride has no effect on kinetics when sodium hydrogen carbonate is present.	34
Methylene blue (MB)	Oxygen	Dioxygen dissolves rapidly [k_{O_2} (dissolution) = $4.1 \times 10^{-2} \text{ min}^{-1}$] in aqueous TiO ₂ , the dispersion exposed to air (12.56 cm ²) to the reaction volume (50.0 cm ²) is relatively large (0.25 in the present instance).	36
Pesticide pyridaben in CTAB	H ₂ O ₂	The time courses of initialized H ₂ O ₂ concentrations in five different runs of irradiating pyridaben without H ₂ O ₂ and with 20, 40, 60, and 80 m MH ₂ O ₂ , respectively.	39
p-nitrosodimethylaniline	NC00 as scavenger in anaerobic condition	The plot shows a more complex behavior together with a lower initial reaction rate in comparison with the O ₂ -free case.	42
	EDTA or Z as scavenger	The two assumptions that k_1 , $h[P] - k_2$, $h[S]$ and k_3 : O_2 , $1 - SKk_1[P]$ made above, i.e., either EDTA or I, play the dominant role, while P scavenges the left electron in effective competition with O ₂ .	
Methyl orange	H ₂ O ₂ , IO ₄ ⁻ and BrO ₃ ⁻ ,	The concentration of MO is above 100 mg/l, but LH kinetic model cannot describe it. IO ₄ ⁻ , BrO ₃ ⁻ , and H ₂ O ₂ can greatly promote the photocatalytic decolorization of MO.	44
Nylon simulated dyestuff effluent	H ₂ O ₂ , Na ₂ S ₂ O ₈	The addition was found to be beneficial since it is increasing the degradation rate.	46

TABLE X. (Continued.)

Target of compound	Anions	Result	Reference
Rhodamine B (RB)	Methyl viologen (MV ²⁺)	The only reaction products of the oxygen-free case are the bleached products with maximum absorption at 224 nm, the characteristic absorption of the aromatic rings of RB.	47
4-hydroxybenzoic acid (4-HBz) and benzamide (Bz)	Cl ⁻	It can be assumed that degradation occurs on the adsorbed carboxylate in one way directly by holes or indirectly by OH ⁻ formed by reaction with adsorbed water molecules.	48
Photoreduction of a metal ion Ag ⁺	Methanol and ethanol	This study confirmed that the extent of photoreduction of metal ions and photodeposition of the metal clusters on metal-oxide surfaces are two processes highly dependent on the nature of the substrate (hole scavenger) being photo-oxidized.	71

J. Effects on kinetic parameters

Antoine *et al.*³⁴ tried to verify if this behavior was consistent with the LH mechanism. According to the LH model, the reaction rate r varies proportionally with the coverage θ as Eq. (8),^{28,88,89}

$$r = k_{LH} \theta = \frac{k_{LH}(K_L C_{eq})}{1 + K_L C_{eq}}, \quad (8)$$

where C_{eq} is the concentration at adsorption equilibrium, K_L is the Langmuir adsorption constant, and k_{LH} is the apparent LH rate constant for the reaction. Then, if we plot $1/r$ versus $1/C_{eq}$, the equation becomes

$$\frac{1}{r} = \frac{1}{K_L k_{LH} C_{eq}} + \frac{1}{k_{LH}}. \quad (9)$$

More generally, we are aware that the introduction of the parameter “light” in the heterogeneous photocatalytic system makes it different from a well-understood heterogeneous catalytic system,

$$r = \frac{-dC}{dt} = k I C_{eq}. \quad (10)$$

In these conditions, reaction is of first order with respect to concentration and the disappearance rate can be expressed as different parameters in (Table XI) process.³⁴ However, the first-order approximation is still correct at low concentrations and the highest reaction rate was obtained at the lowest pH. The factors affecting degradation are dosage of catalyst, flow rates, and UV radiation intensity tilted angle of the reactor.^{91,92}

V. TYPE OF PHOTOCATALYTIC REACTORS

The photocatalysis can be carried out in various reactors. There are many types of reactors that can be used in the photocatalytic studies. The selection normally depends on the experimental conditions and applications. The designs of the photoreactor depend on geometry, texture of the catalyst, and optical pathway. Reactors can be briefly classified in two types: reactors that use a catalyst as suspension form and reactors that use a thin film catalyst. Both kinds of reactors can be designed as an immersion well or flat wall. Immersion well photoreactors are normally used at laboratory scale for evaluation purposes.⁹ Several reactors have been described, e.g., tanks with suspended matter (in water or in air), tanks with immobilized photocatalyst, agitators, tubes, or pools. Titanium dioxide layer can cover reactor walls, surfaces of reactor packing, outer surfaces of some exposure lamps, and rotors placed inside the reactors.⁹³⁻⁹⁹ A number of photocatalytic reactors have been patented in recent years. Based on the catalyst used, light source and the reactor vessel, all photocatalytic reactor configurations fall under four categories. They are slurry-type, immersion-type with lamps,¹⁰⁰ external-type with lamps (outside the reactor),¹⁰¹ and distributive-type with the light by optical means, such as reflectors and light conductors¹⁰⁰ or optical fibers.¹⁰² The reactors are helical, spiral, shallow cross-flow basins or optical fiber. However, all these reactor designs are limited to small scales by the low values of the key parameter k . An external-type reactor will always be limited by low values of k . An immersion-type reactor could be scaled-up to any dimension, but when classical lamps of a diameter between 0.07 and 0.1 m are used, the k value is very low even if it is assumed that the lamps occupy 75% of the reactor volume. Many other innovative-type reactor designs exist in literature addressing specific problems and applications or being designed especially for treating specific types of pollutants.¹⁰³ In this section (Table XII), we highlight the studies on various reactor designs and their treatment efficiencies. For the nonconcentrating systems, estimates have concluded that solar photons can be used at a lower cost than photons from UV lamps.²⁸ The treatments of biologically pretreated wastewater from a textile factory and car washing unit were successfully carried out with artificial light and sunlight.¹⁰⁶ A comparison has also been made among thin-film fixed-bed reactors, para-

TABLE XI. (Continued.)

Target of compound	pH studied	Initial concentration	Photocatalyst	Light source	Ions/anion/electron acceptors/hole scavengers	Temperature	Effect of A/V ratio and flow rate	Reference
Methylene blue (MB)	Pseudo-first-order kinetics even at high initial concentrations of MB (0.3 mM).		Total accumulated light energy absorbed by the TiO ₂ particles, but increased proportionately with increase in light irradiance.	36
4BS azo dye		Increased concentration of dye per volume increase. At the same reaction time, decolorization decreases.	The introduction of illumination intensity to the kinetic model.	The volume is $50.0 \times 10^{-6} \text{ m}^3$ and the irradiation area is $3.92 \times 10^{-5} \text{ m}^2 \text{ m}^{-3}$	At increased stirring speeds, the bulk solution much improved.	37
Benzoic acid, phenol, and salicylic acid	$k=0.15 \text{ h}^{-1} (t^{1/2}=4.5 \text{ h, pH 5})$, $k=0.15 \text{ h}^{-1} (t^{1/2}=4.6 \text{ h, pH 7})$, and $k=0.20 \text{ h}^{-1} (t^{1/2}=3.4 \text{ h, pH 9})$. Fast degradation at pH 9 for salicylic acid.	The relevant dynamics of desorption in the f benzoic acid are $k=0.004 \text{ h}^{-1} (\text{pH 9})$, $k=0.17 \text{ h}^{-1} (\text{pH 7})$, and $k=0.10 \text{ h}^{-1} (\text{pH 5})$	41
p-nitrosodimethylaniline	The trapped whole at TiO surface is similar in oxidizing power to the OH-radical in solution.	As inferred from the plot, it shows a more complex behavior together with a lower initial reaction rate in comparison with the O ₂ -free case.	The lower rate constant infers a less reactivity of the trapped electron compared with the free one.	Zero-order rate constant $2 Zk$, $h[S]/[k, +k, h[S]$	42

TABLE XI. (Continued.)

Target of compound	pH studied	Initial concentration	Photocatalyst	Light source	Ions/anion/electron acceptors/hole scavengers	Temperature	Effect of A/V ratio and flow rate	Reference
Methyl orange	Zero-order rate constant first-order pseudo-first-order rate constant	The decolorization of MO increases with the increasing of the dosage of the catalyst.	The dosage of the catalyst is 5 g l^{-1} , the decolorization of MO is up to 100%.	$\ln(C_0/C_t)$ versus t gives decolorization rate constant.	C_t versus t is in linear that fits a zero order that is $C_t = C_0 - k_0 t$	44
DBS (ZnO), KS (ZnO), DBS (TiO ₂), BS (TiO ₂)	A TiO ₂ or ZnO is possibly applicable to all sulfur-containing organic compounds.	45
4-hydroxy benzoic acid (4-HBz) and benzamide(Bz)	Between pH 4 and 8, there is no variation of the degradation rate of Bz pure solution.	However, the kinetic of amide mineralization is slower, which explains the shallower slope.	Pseudo-first-order rate constants k_0 (min^{-1}) different pH with $[\text{TiO}_2]_0^{1/4} \text{ g l}^{-1}$	More sensitive to presence of chlorides.	48
4-nitrophenol in aqueous	At $\text{pH} > \text{pK}_a$ and at $\text{pH} < \text{pK}_a$. Similarly, the catalyst surface is negatively charged at $\text{pH} > \text{pH}_{zpc}$ and positively charged at $\text{pH} < \text{pH}_{zpc}$.		The increasing branch ($[\text{Ti}] < 4 \text{ g dm}^{-3}$) can be described by a power-law relationship ($k_0 = A [\text{Ti}]^b$) with $b = 0.384$.	Irradiating power maximum value in about 2 min after switching on the lamp			The relevant heat of adsorption ($\Delta H = -18.8 \text{ kJ mole}^{-1}$)	90

TABLE XII. Performance of photocatalytic reactors.

Target of compound	Type of reactors/capacity	Flow rate	Result	Reference
C.I. reactive red 198	A 3 L, hollow cylindrical glass reactor using a 500 W medium-pressure, 300 mW cm ⁻² Hg lamp (254 nm) inside a quartz tube	...	During decolorization some Cl ⁻ , NO ₃ ⁻ , and SO ₄ ²⁻ ions were released and, even TOC was reduced by only 50%.	3
Acridine orange	The 15 W UV-365 nm tubes positioned on two sides of the cabinet interior. A water system, equipped with a binary pump, a photodiode array detector, an autosampler, and a micromass detector, was used for separation and identification.	...	Decolorized and degraded by TiO ₂ under UV irradiation, after 15 W UV-365 nm irradiation for 24 h, ~99.7% of AO was degraded.	5
Azo dye acid red 114	For the UV/photocatalyst process, irradiation was performed in a batch reactor of 2 L in volume with an Hg lamp Philips of 32 W.	...	The SSD method is an effective method for supporting TiO ₂ on CP.	8
Azo dye (AR27)	A mercury UV lamp (30 W, UV-C, $\lambda_{\text{max}}=254$ nm) which was placed above a 500 ml jacket Pyrex glass reactor.	...	The power law-type rate expression is in good agreement with the experimental data.	13
DN SDA, ANS DA, and DASDA	A UV lamp (300–450 nm), power consumption of 15 W, was used; the suspension of TiO ₂ was maintained by magnetic stirring and bubbling the air from the top of the reactor.	...	DASDA, containing two amino groups, disappeared very quickly by both the techniques followed by ANSDA with one amino- and one nitro-group and DNSDA with two nitro groups.	30
Chrysoidine Y	A 125 W medium pressure mercury lamp and Pyrex glass equipped with a magnetic stirring bar, a water-circulating jacket, and oxygen were used.	...	A high degradation rate, which is essential for any practical application of photocatalytic oxidation processes.	31
2-chlorophenol	1.5 L capacity, a 100 W mercury lamp, filled with 1 L of 12.5–75 mg/l solution with 10–50 mg/l of Co-doped TiO ₂ nanoparticles.	...	The efficiency values of the 2-CP photodegradation were 93.4% and 96.4% at solution pH of 9 and 12, respectively.	51
Chlorobenzene	A 125 W UV lamp with $\lambda_{\text{max}} 365$ nm was used. Air was bubbled at sufficiently high velocity (>2 cm s ⁻¹) to keep all the TiO ₂ in suspension.	...	The rate of degradation is faster with UV radiation than with concentrated solar radiation.	62
Naphthalene	A 125 W lamp, titanium 25 ml, T=20 °C, pH=4.4 dye concentration=5 ppm/40 μ M. Mass concentration of suspended TiO ₂ =2.5 g/l, $\lambda=365$ nm. Efficient photonic flux $\phi=5.4 \times 10^{15}$ photons s ⁻¹	...	The presence of carbonates and hydrogen carbonates was found to inhibit adsorption and degradation of naphthalene, whereas sodium chloride at pH < pHPzc accelerates the reaction through adsorption enhancement.	34

TABLE XII. (Continued.)

Target of compound	Type of reactors/capacity	Flow rate	Result	Reference
Benzene derivatives	Pyrex glass containers of 50 ml closed with septa as cylindrical batch photoreactors. Illumination was performed with a xenon lamp in a CPS Sun test system at 550 W/m ² light intensity (AM1) with a filter that cuts off wavelengths below 290 nm.	...	The results showed that IEP seems to influence significantly organic degradation. Indeed, TiO ₂ catalysts with an acidic IEP accelerate organic compound degradation.	35
Methylene blue (MB)	The solution (50 ml) containing MB (0.1 mM) and 100 mg of TiO ₂ . 75 W Hg lamp, wavelength range of 310–400 nm (λ max=360 nm)	...	Maximal absorbance at 668 and 609 nm. Under experimental, maximal absorption occurred at 664 and 612 nm at pHs 1–7.	36
Winery wastewater	An annular type reactor, capacity is 60 L with an irradiated volume of 38.5 L. The outer chamber is a stainless steel vessel (inside diameter=30 cm, height =60 cm), fitted UV lamp enclosed in a cylindrical quartz tube (inside diameter=5 cm), a UV lamp range (310–435 nm), with peak at 365 nm.	0–10 L/min	The highest photodegradation rate and the maximum COD removal were achieved at zero catalyst loading with COD removal of about 84%.	38
RY17, RB4, and RR2	Using 6 × 8 W low-pressure mercury arc lamp (254 nm) built into lamp housing with polished anodized aluminum reflectors and placed 6.5 cm away from the reactor in order to prevent light radiation.	...	6 h UV irradiation whereas complete degradation requires more than 10 h in solar irradiation of RY17 dye. Similar observations are made in the case of RR2 and RB4 and the results.	43
DBS (ZnO), KS (ZnO), DBS (TiO ₂), BS (TiO ₂)	A 100 W Hg lamp, a 100 ml glass vessel, the TiO ₂ or ZnO particles (100 mg) and 50 ml of aqueous solution (0.1 mM), initial concentration (0.1 mM, 20.6 mg/l).	...	When the compounds that contained a benzene ring were degraded, SO ₄ ²⁻ ion production reached an equilibrium condition in short time.	45
Nylon simulated dyestuff effluent (NSW)	Collector (ACPC=3.09 m ²) has eight Pyrex tubes connected in series and mounted on a fixed platform inclined at a 37° angle, irradiation (300–400 nm), flows at 20 L/min.	20 L/min	Initial organic carbon content of 0.15 g l ⁻¹ (0.5 g l ⁻¹ COD) and 0.15 g/l (0.55 g/l COD) for NSW and CSW, respectively.	46
Benzidine-based azo dyes	The system was 3 L, a Pyrex glass tube having 100 cm in length and 2.54 cm of internal diameter, located in the focus of the CPC collector.	...	Decolorization decreased to 56% under the same reaction conditions and a COD removal up to almost 63% was achieved.	104
MB or RB	The volume of the photoreactor (36 cm l × 27.5 cm W × 8 cm H) was approximately 8.0 L, three 15 W low-pressure Hg lamps.	70 rpm	Hydrolysis, hydroxylation, and quinonation were the major for decomposing carbaryl in such a photocatalytic system.	105

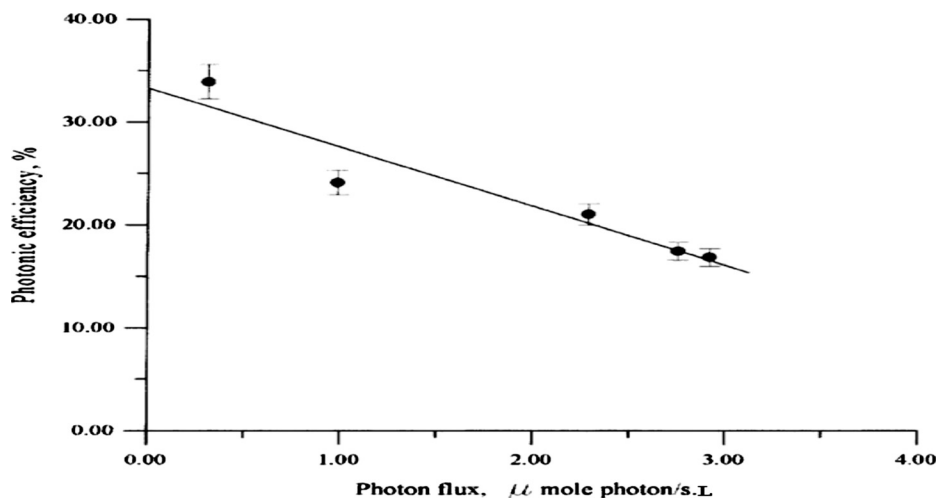


FIG. 6. The photonic efficiency against the calculated photon flux.

bolic trough collectors, and plexiglass double-skin sheet reactors.¹⁰⁷ A reactor designed and constructed based on the modeling results was reported to show promising results.¹⁰³

VI. ECONOMIC ANALYSIS OF PHOTOCATALYTIC SYSTEM

This unit discusses the main factors entering into the cost of solar detoxification systems and describes how to go about the economic assessment of specific solar photocatalytic applications. More efficient systems have been designed that ultimately aimed for an overall increase in efficiency and decrease in cost. The cost of the early solar technology is higher than for the more mature competitors. However, several areas that are actively being pursued promise substantial improvements that should reduce costs for the detoxification system below those for the alternatives.¹⁰⁸ It may vary on a wide range according (i) to the nature of the catalyst, (ii) to the experimental conditions used (concentrations, T, m), and (iii) especially to the nature of the reaction considered. We have found values that comprised between 10–2 and 70%. The knowledge of this parameter is fundamental. It enables one (i) to compare the activity of different catalysts for the same reaction, (ii) to estimate the relative feasibility of different reactions, and (iii) to calculate the energetic.²⁸ Economic analysis of photocatalytic system should include evaluating the economic value of autocatalytic processes.

A. Photonic efficiency

The effect of light intensity on the photonic efficiency of the photocatalytic degradation of KHP using Degussa P25 is illustrated in Fig. 6. The efficiency decreased considerably as the light intensity increased due to the high recombination rate at high light intensities. This makes the photocatalytic oxidation reaction less effective. The maximum photonic efficiency value reached was 33.9%, which was remarkably high in comparison to literature data for other model pollutants.²⁷ The photonic efficiency can be calculated by^{109,110}

$$\zeta = \frac{R}{I_0}, \quad (11)$$

where R is the initial rate of concentration degradation ($\text{mol l}^{-1} \text{min}^{-1}$) and I_0 is the incident photon flux ($\text{Einstein m}^{-2} \text{s}^{-1}$).

B. Energy yield

The energy yield can be calculated by

$$EY(\text{g/kW h}) = \frac{([C]_{\text{in}} - [C]_{\text{out}}) \times M \times Q \times 3600}{V_M \times P \times 1000}, \quad (12)$$

where $[C]_{\text{in}}$ and $[C]_{\text{out}}$ are the chemical concentration of odorous compound at the inlet and outlet of the odor treatment (in ppm), M is the molar mass of the compound (in g/mole), Q is the gas flow rate (in l/s), and V_M is the molar volume of the gas (in L/mole) in the experiments (atmospheric pressure, ambient temperature) $V_M=24.04$ l/mole. P is the power of the microwave (in watt).¹¹¹

C. Operating cost

The sum of personnel, maintenance materials, electricity, and chemical supplies is the total operating cost of the solar detoxification system. The annual levelized cost and treatment cost per m^3 of treated wastewater can be calculated as⁵³

$$\text{Annual Levelized Cost} = \text{Total Installed Cost} \times \text{FCR} + \text{Operating Cost}, \quad (13)$$

$$\text{Treatment Cost}(\text{Euros}/\text{m}^3) = \frac{\text{Annual Cost}}{\text{Annual Treatment Capacity}}. \quad (14)$$

The fixed charge rate is normally equal to the sum of the return on debit, taxes, depreciation, insurance, etc. For solar detoxification treatment plants, a plant life of 12 years with a depreciation period of ten years may normally be assumed. A field test for detoxification of water contains benzene, toluene, ethyl benzene, and xylene pollutants. The treatment cost was estimated to be \$5.52/1000 gal, and the authors reported that such costs are competitive with those of conventional treatment technologies. The analysis was said to be preliminary and require long-term testing to determine the actual costs of pretreatment and catalyst life.¹¹² Costs for a solar system at the site were found to be high (\$18–26/1 m^2 or \$70–100/1000 gal). Three different solar operating configurations explored for the treatment of 100 000 gal/day of groundwater contaminated with trichloroethylene. They concluded that the current projected costs for solar water detoxification systems were comparable with those for conventional treatment technologies such as carbon adsorption and electric lamp-powered, ultraviolet light/hydrogen peroxide systems. In another study which suggested that the largest gains (perhaps 5–100 times) for a designed fixed-bed parabolic trough reactor could be made through catalyst improvements and system cost reductions (3–4 times) and process optimization (1.5–2 times) would likely be smaller. A preliminary comparison of process economics between ultraviolet ozonation and activated carbon adsorption using a reference of integrated water treatment for the removal of pollution control boards. Their calculations indicated that all intermediate and larger sizes of reactors, the costs of photocatalytic systems, are comparable to those of activated carbon systems.²³

VII. RESULTS AND DISCUSSION

In this comprehensive paper, the treatment of hazardous wastewater bearing organic compounds by photocatalysis and the effects of various parameters such as pH, mass of catalyst, initial concentration, wavelength, electron acceptor, temperature and radiant flux, light intensity, etc. are reviewed. Tables I–XII summarize the results studied on different parameters performed on increasing and decreasing order. In addition, the design features and efficiencies of various photo-reactors used for this process are also discussed for the treatment of industrial wastewater. However, a lot more is needed from engineering design and modeling for successful application of the laboratory scale techniques to large-scale operation. To summarize this review the following discussion points can be made.

- (i) The results of the photodegradation rate of advanced oxidation in maximum pollutant compounds as a function of reaction pH showed that the rate of degradation proceeded much faster at alkaline pH values.

- (ii) With increase in pH, the initial rate of degradation and adsorption decreases while both increase with decrease in pH, indicating that pH is an important factor significantly affecting adsorption and the corresponding initial rate of degradation. The lowering of the degradation rate at high pH levels can be explained by the adsorption-desorption effect. But in some cases the highest reaction rate was obtained at the lowest pH. In highly acidic medium, the rate of degradation was high and decreased as the pH of the solution was increased up to 11.
- (iii) It is also evident that the effect of photodegradation efficiency and decolorization reaction becomes faster when increases with an increase in the amount of photocatalyst and the results indicate that initial rate of photodegradation increases with increase in catalyst dose up to an optimum loading, further increase in catalyst dose showed no effect.
- (iv) On increasing the initial concentration of dye, more and more dye molecules are adsorbed on the surface of TiO₂.
- (v) The increase in the photonic flux does not induce a proportional increase in the degradation rate, but that the difference in the rate of degradation is attributed to difference in the input energy.
- (vi) The additions of ions/electron acceptors/oxidizing reagent were found to be beneficial since it is increasing the degradation rate.
- (vii) Using the sun as a light source introduces new process requirements that deal with the intermittent nature of this source of photons.

VIII. CONCLUSIONS

The solar/UV radiations can be used to decompose organic matters, which have many environmental and industrial applications. Key variables for achieving this goal include the optimization of mass-transfer rates, light penetration, the UV source, and H₂O₂ deployment. By applying the optimal experimental conditions, obtained from the different types of model experiments to the real wastewater samples for improvements, the catalytic process is possible with the use of better UV lamps and the development of higher performance catalysts. The present treatment costs of photocatalytic systems are slightly higher than those of conventional techniques, but the efforts being made in the design of more efficient systems with improved catalyst usage will establish this technology to be a cleaner and cost effective alternative. It is likely that cost-competitive solar technologies for environmental clean-up applications will become commercially available in the next few years. This study investigates the effect of the various parameters on the treatment cost for different reactor types. The resulting combined processes revealed a flexible line of action for the treatment technologies and the choice of treatment method usually depends upon the composition of industrial wastewater.

ACKNOWLEDGMENTS

The authors are thankful to Rajiv Gandhi National Fellowship M.Phil./Ph.D. from University Grant Commission, Delhi (India), for providing the financial support for the research, and also to Energy and Environmental Studies, Devi Ahilya University, Indore for giving the opportunity for this research work.

¹M. V. Alexander and J. J. Rosentreter, *Microchem. J.* **88**, 38 (2008).

²S. Malato, J. A. Blanco, A. Vidal, A. O. Diego, M. I. Maldonado, J. C. Aceres, and W. Gernjak, *Sol. Energy* **75**, 329 (2003).

³C.-H. Wu, *Dyes Pigm.* **77**, 31 (2008).

⁴M. Saquib, M. A. Tariq, M. Faisal, and M. Muneer, *Desalination* **219**, 301 (2008).

⁵C.-S. Lu, F.-D. Mai, C.-W. Wu, R.-J. Wu, and C.-C. Chen, *Dyes Pigm.* **76**, 706 (2008).

⁶A. K. Ray, *Catal. Today* **44**, 357 (1998).

⁷K. Kabra, R. Chaudhary, and R. L. Sawhney, *Ind. Eng. Chem. Res.* **43**, 7683 (2004).

⁸M. Nikazar, K. Gholivand, and K. Mahanpoor, *Desalination* **219**, 293 (2008).

⁹R. A. Al-Rasheed, "Water treatment by heterogeneous photocatalysis: An overview," presented at the Fourth SWCC Acquired Experience Symposium, Jeddah, 2005.

¹⁰F. Mollers, H. J. Tolle, and R. Memming, *J. Electrochem. Soc.* **121**, 1160 (1974).

¹¹U. I. Gaya and A. H. Abdullah, *J. Photochem. Photobiol. C* **9**, 1 (2008).

- ¹² D. M. Blake, "Solar Processes for the Destruction of Hazardous Chemicals," in *Alternative Fuels and the Environment*, edited by F. Sterrett (CRC Press, Lewis Publishers, Boca Raton, 1994), pp. 175.
- ¹³ M. A. Behnajady, N. Modirshahla, and H. Fathi, *J. Hazard. Mater.* **136**, 816 (2006).
- ¹⁴ I. Losito, A. Amorisco, F. Palmisano, and P. G. Zamboni, *Appl. Surf. Sci.* **240**, 180 (2005).
- ¹⁵ S. B. Sankapal, M. C. Steiner, and A. Ennaoui, *Appl. Surf. Sci.* **239**, 165 (2005).
- ¹⁶ C. H. Kwon, H. Shin, J. H. Kim, W. S. Choi, and K. H. Yoon, *Mater. Chem. Phys.* **86**, 78 (2004).
- ¹⁷ J. H. Yang, Y. S. Han, and J. H. Choy, *Thin Solid Films* **495**, 266 (2006).
- ¹⁸ Z. Ding, X. Hu, P. L. Yue, G. Q. Lu, and P. F. Greenfield, *Catal. Today* **68**, 173 (2001).
- ¹⁹ H. D. Nam, B. H. Lee, S. Kim, C. Jung, J. Lee, and S. Park, *J. Appl. Phys.* **37**, 4063 (1998).
- ²⁰ S. E. Pratsinis, *J. Aerosol Sci.* **27**, S153 (1996).
- ²¹ S. Sen, S. Mahanty, S. Roy, O. Heintz, S. Bourgeois, and D. Chaumont, *Thin Solid Films* **474**, 245 (2005).
- ²² B. Guo, Z. Liu, L. Hong, H. Jiang, and J. Y. Lee, *Thin Solid Films* **479**, 310 (2005).
- ²³ D. F. Ollis, E. Pelizzetti, and N. Serpone, *Environ. Sci. Technol.* **25**, 1522 (1991).
- ²⁴ O. Carp, C. L. Huisman, and A. Reller, *Prog. Solid State Chem.* **32**, 33 (2004).
- ²⁵ T. Ohno, K. Sarukawa, K. Tokieda, and M. Matsumura, *J. Catal.* **203**, 82 (2001).
- ²⁶ A. P. Toor, A. Verma, C. K. Joshi, P. K. Bajpai, and V. Singh, *Dyes Pigm.* **68**, 53 (2006).
- ²⁷ G. Alhakimi, L. H. Studnicki, and M. Al-Ghazali, *J. Photochem. Photobiol., A* **154**, 219 (2003).
- ²⁸ J.-M. Herrmann, *Catal. Today* **53**, 115 (1999).
- ²⁹ A. Riga, K. Soutsas, K. Ntampeliotis, V. Karayannis, and G. Papapolymerou, *Desalination* **211**, 72 (2007).
- ³⁰ R. N. Rao and N. Venkateswarlu, *Dyes Pigm.* **77**, 590 (2008).
- ³¹ M. Qamar, M. Saquib, and M. Muneer, *Desalination* **171**, 185 (2005).
- ³² J. Papp, S. Soled, K. Dwight, and A. Wold, *Chem. Mater.* **6**, 496 (1994).
- ³³ G. Takei, T. Kitamori, and H.-B. Kim, *Catal. Commun.* **6**, 357 (2005).
- ³⁴ L. Antoine, F. Corinne, C. Jean-Marc, and H. Jean-Marie, *J. Photochem. Photobiol., A* **193**, 193 (2008).
- ³⁵ L. Rizzo, J. Koch, V. Belgiorno, and M. A. Anderson, *Desalination* **211**, 1 (2007).
- ³⁶ T. Zhang, T. Oyama, A. Aoshima, H. Hidaka, J. Zhao, and N. Serpone, *J. Photochem. Photobiol., A* **140**, 163 (2001).
- ³⁷ X. Yin, F. Xin, F. Zhang, S. Wang, and G. Zhang, *Environ. Eng. Sci.* **23**, 1000 (2006).
- ³⁸ T. E. Agustina, H. M. Ang, and V. K. Pareek, *Chem. Eng. J.* **135**, 151 (2008).
- ³⁹ X. Zhu, C. Yuan, and H. Chen, *Environ. Sci. Technol.* **41**, 263 (2007).
- ⁴⁰ C. Sriwong, S. Wongnawa, and O. Patarapaiboolchai, *Catal. Commun.* **9**, 213 (2008).
- ⁴¹ H. Hidaka, H. Honjo, S. Horikoshi, and N. Serpone, *Catal. Commun.* **7**, 331 (2006).
- ⁴² L. Zang, P. Qu, J. Zhao, T. Shen, and H. Hidaka, *J. Mol. Catal. A: Chem.* **120**, 235 (1997).
- ⁴³ B. Neppolian, H. C. Choi, S. Sakthivel, B. Arabindoo, and V. Murugesan, *J. Hazard. Mater.* **89**, 303 (2002).
- ⁴⁴ Z. Junbo, M. Di, Z. Hong, L. An, L. M. Jiao, H. Shengtian, and L. Jianzhang, *Cent. Eur. J. Chem.* **6**, 245 (2008).
- ⁴⁵ H. Hidaka, K. Nohara, K. Oishi, J. Zhao, N. Serpone, and E. Pelizzetti, *Chemosphere* **29**, 2619 (1994).
- ⁴⁶ M. Kositz, A. Antoniadis, I. Poullos, I. Kiridis, and S. Malato, *Sol. Energy* **77**, 591 (2004).
- ⁴⁷ P. Qu, J. Zhao, T. Shen, and H. Hidaka, *J. Mol. Catal. A: Chem.* **129**, 257 (1998).
- ⁴⁸ D. Robert, A. Piscopo, and J. V. Weber, *Sol. Energy* **77**, 553 (2004).
- ⁴⁹ G. Colon, M. C. Hidalgo, J. A. Navio, E. Pulido Melian, O. Gonzalez Diaz, and J. M. Dona, *Appl. Catal., B* **78**, 176 (2008).
- ⁵⁰ F. Kiriakidou, D. I. Kondarides, and X. E. Verykios, *Catal. Today* **54**, 119 (1999).
- ⁵¹ M. A. Barakat, H. Schaeffer, G. Hayes, and S. Ismat-Shah, *Appl. Catal., B* **57**, 23 (2005).
- ⁵² S. Jian-Wen, Z. Jing-Tang, H. Yan, and Z. Yu-Cui, *Mater. Chem. Phys.* **106**, 247 (2007).
- ⁵³ J. B. Galvez and S. M. Rodriguez, *Solar Detoxification* (Electronic copy, United Nations Educational, Scientific and Cultural Organization, 2003), pp. 1–246.
- ⁵⁴ S. K. Kansal, M. Singh, and D. Sud, *Indian Institute of Chemical Engineers* **49**, 11 (2007).
- ⁵⁵ H. Lu, M. A. Schmidt, and K. F. Jensen, *Lab Chip* **1**, 22 (2001).
- ⁵⁶ K. Ueno, F. Kitagawa, and N. Kitamura, *Lab Chip* **2**, 231 (2002).
- ⁵⁷ R. Gorges, S. Meyer, and G. Kreisel, *J. Photochem. Photobiol., A* **167**, 95 (2004).
- ⁵⁸ H. Nakamura, X. Li, H. Wang, M. Uehara, M. Miyazaki, H. Shimizu, and H. Maeda, *Chem. Eng. J.* **101**, 261 (2004).
- ⁵⁹ T. Fukuyama, Y. Hino, N. Kamata, and I. Ryu, *Chem. Lett.* **33**, 1430 (2004).
- ⁶⁰ K. Jahnisch and U. Dingerdissen, *Chem. Eng. Technol.* **28**, 426 (2005).
- ⁶¹ Y. Matsushita, S. Kumada, K. Wakabayashi, K. Sakeda, and T. Ichimura, *Chem. Lett.* **35**, 410 (2006).
- ⁶² Y. Matsushita, N. Ohba, S. Kumada, K. Sakeda, T. Suzuki, and T. Ichimura, *Chem. Eng. J.* **135**, S303 (2008).
- ⁶³ D. S. Bhatkhande, S. B. Sawant, J. C. Schouten, and V. G. Pangarkar, *J. Chem. Technol. Biotechnol.* **79**, 354 (2004).
- ⁶⁴ M. N. Rashed and A. A. El-Amin, *Int. J. Phys. Sci.* **2**, 073 (2007).
- ⁶⁵ M. Sameiro, T. Gonçaves, E. M. S. Pinto, P. Nkeonye, and A. M. F. Oliveira-Campos, *Dyes Pigm.* **64**, 135 (2005).
- ⁶⁶ S. Mozia, M. Tomaszewska, and A. W. Morawski, *Desalination* **185**, 449 (2005).
- ⁶⁷ L. Chin-Chuan, H. Yung-Hsu, L. Pao-Fan, L. Chia-Hsin, and K. Chao-Lang, *Dyes Pigm.* **68**, 191 (2006).
- ⁶⁸ A. Mills, R. H. Davies, and D. Worsley, *Chem. Soc. Rev.* **22**, 417 (1993).
- ⁶⁹ W. S. Struve, *Fundamentals of Molecular Spectroscopy* (Wiley & Sons, New York, 1989).
- ⁷⁰ P. W. Atkins, *Molecular Quantum Mechanics*, 2nd ed. (Oxford University Press, Oxford, U.K., 1983).
- ⁷¹ H. Hidaka, H. Honjo, S. Horikoshi, and N. Serpone, *Sens. Actuators B* **123**, 822 (2007).
- ⁷² N. Serpone, J. Martin, S. Horikoshi, and H. Hidaka, *J. Photochem. Photobiol., A* **170**, 51 (2005).
- ⁷³ A. R. Nicolaescu, O. Wiest, and P. V. Kamat, *J. Phys. Chem. A* **109**, 2829 (2005).
- ⁷⁴ I. K. Konstantinou and T. A. Albanis, *Appl. Catal., B* **49**, 1 (2004).
- ⁷⁵ N. Daneshvar, D. Salari, and A. R. Khataee, *J. Photochem. Photobiol., A* **157**, 111 (2003).
- ⁷⁶ M. Muruganandham and M. Swaminathan, *Dyes Pigm.* **68**, 133 (2006).
- ⁷⁷ M. Faisal, M. A. Tariq, and M. Muneer, *Dyes Pigm.* **72**, 233 (2007).
- ⁷⁸ N. Shimizu, C. Ogino, M. F. Dadjour, and T. Murata, *Ultrason. Sonochem.* **14**, 184 (2007).
- ⁷⁹ N. M. Mahmoodi, M. Arami, and N. Y. Limaee, *J. Hazard. Mater.* **133**, 113 (2006).

- ⁸⁰M. Carrier, N. Perol, J. M. Herrmann, C. Bordes, S. Horikoshi, and J. O. Paise, *Appl. Catal., B* **65**, 11 (2006).
- ⁸¹B. Viswanathan, *Bull. Catal. Soc. India* **2**, 71 (2003).
- ⁸²S. Irmak, E. Kusvuran, and O. Erbatır, *Appl. Catal., B* **54**, 85 (2004).
- ⁸³N. San, A. Hatipoglu, G. Koçtürk, and Z. Çýnar, *J. Photochem. Photobiol., A* **146**, 189 (2002).
- ⁸⁴A. Syoufian and K. Nakashima, *J. Colloid Interface Sci.* **317**, 507 (2008).
- ⁸⁵J. P. A. Benjamin, B. Cornish, L. A. Lawton, and P. K. Robertson, *Appl. Catal., B* **25**, 59 (2000).
- ⁸⁶H. de Lasa, B. Serrano, and M. Salaices, *Photocatalytic Reaction Engineering* (Springer, New York, 2005).
- ⁸⁷C. S. Turchi, M. S. Mehos, and H. F. Link, "Design and cost of solar photocatalytic systems for groundwater remediation," NREL Technical Paper No. 432-4865, May 1992.
- ⁸⁸T. Ichimura, Y. Matsushita, K. Sakeda, and T. Suzuki, in *Microchemical Engineering in Practice*, edited by T. R. Dietrich (Wiley-Blackwell, John Wiley & Sons, Inc., New Jersey, 2009), pp. 487.
- ⁸⁹J.-M. Herrmann, M. N. Mozzanega, and P. Pichat, *J. Photochem.* **22**, 333 (1983).
- ⁹⁰R. Andreatti, V. Caprio, A. Insola, G. Longo, and V. Tufano, *J. Chem. Technol. Biotechnol.* **75**, 131 (2000).
- ⁹¹J. Giménez, M. A. Aguado, and S. Cervera-March, *J. Mol. Catal. A: Chem.* **105**, 67 (1996).
- ⁹²J. Inamdar and S. K. Singh, *Int. J. Natural Sci. and Eng.* **1**, 4 (2008).
- ⁹³R. Masuda, K. Kitamura, and K. Kawashima, "Treatment of trichloroethylene—Containing wastewater and photocatalytic apparatus," Japanese Kokai Tokkyo Koho Patent No. JP 08 323,347 (1996).
- ⁹⁴R. Masuda, K. Kitamura, S. Yamashita, and K. Kawashima, "Dry cleaning wastewater treatment and photocatalytic apparatus," Japanese Kokai Tokkyo Koho Patent No. JP 08 323-346 (1996).
- ⁹⁵K. Sato, "Photoactive water treatment agents and containers for them," Japanese Kokai Tokkyo Koho Patent No. JP 10 34,143 (1998).
- ⁹⁶H. Majima, T. Kurihara, and S. Nagaoka, "Photocatalysts and their manufacture and usage," Japanese Kokai Tokkyo Koho Patent No. JP 10 249,210 (1998).
- ⁹⁷R. Franke, "Reactor for water treatment and method for photocatalytic decomposition of chemicals in water and wastewaters," German Offen. Patent No. DE 19 806,331 (1998).
- ⁹⁸H. Zota and J. Arai, "Apparatus for treatment of air and water by photocatalyst," Japanese Kokai Tokkyo Koho Patent No. JP 09 314,137 (1997).
- ⁹⁹Y. Kamitani and T. Takemura, "Process and apparatus for (waste) water treatment," Japanese Kokai Tokkyo Koho Patent No. JP 10 263,534 (1998).
- ¹⁰⁰A. K. Ray, *Catal. Today* **40**, 73 (1998).
- ¹⁰¹J. W. Assink, T. P. M. Koster, and J. M. Slaager, "Fotokatalytische oxydatie voor afvalwater behandeling," Internal Report Ref. No. 93 ± 137, TNO ± Milieu en Energie, Apeldoorn, The Netherlands, 1993.
- ¹⁰²N. J. Peill and M. R. Hoffmann, *Environ. Sci. Technol.* **29**, 2974 (1995).
- ¹⁰³A. K. Ray, *Chem. Eng. Sci.* **54**, 3113 (1999).
- ¹⁰⁴K. Chiang, R. Amal, and T. Tran, *Adv. Environ. Res.* **6**, 471 (2002).
- ¹⁰⁵W. S. Kuo, Y. H. Chiang, and L. S. Lai, *Dyes Pigm.* **76**, 82 (2008).
- ¹⁰⁶W. Xi, S.-U. Geissen, and A. Vogelppohl, *Water Sci. Technol.* **44**, 237 (2001).
- ¹⁰⁷R. Goslich, R. Dillerty, and D. Bahnemann, *Water Sci. Technol.* **35**, 137 (1997).
- ¹⁰⁸J. V. Anderson, H. Link, M. Bohn, and B. Gupta, *Sol. Energy Mater.* **24**, 538 (1991).
- ¹⁰⁹M. Muneer and D. Bahnemann, *Appl. Catal., B* **36**, 95 (2002).
- ¹¹⁰A. Chatzidakis, C. Berberidou, I. Paspaltsis, G. Kyriakou, T. Sklaviadis, and I. Poullos, *Water Res.* **42**, 386 (2008).
- ¹¹¹J. Jarrig and P. Vervisch, *Plasma Chem. Plasma Process.* **27**, 241 (2007).
- ¹¹²J. C. Crittenden, Y. Zhang, D. W. Hand, D. L. Perram, and E. G. Marchand, *Water Environ. Res.* **68**, 270 (1996).